N O T I C E

NASA Contract Report 165137

Final Report

Influence of Mistuning on Blade Torsional Flutter

A.V. Srinivasan

UNITED TECHNOLOGIES RESEARCH CENTER
East Hartford, CT 06108

N80-31351

(NASA-CR-165137)   INFLUENCE OF MISTUNING ON
BLADE TORSIONAL FLUTTER (United Technologies
Research Center)   55 p HC A04/MF A01
                                          CSCL 01A   Unclas
                                                  G3/02   28590

NASA

National Aeronautics and
Space Administration

Lewis Research Center
Cleveland, Ohio 44135

SEP 1980
RECEIVED
NASA STI FACILITY
ACCESS DEPT.

1. Report No. CR-165137	2. Government Accession No.	3. Recipient's Catalog No.
4. Title and Subtitle INFLUENCE OF MISTUNING ON BLADE TORSIONAL FLUTTER		5. Report Date August 1980
		6. Performing Organization Code
7. Author(s) A. V. Srinivasan		8. Performing Organization Report No. R80-914545-16
		10. Work Unit No.
9. Performing Organization Name and Address United Technologies Research Center Silver Lane East Hartford, CT. 06108		
		11. Contract or Grant No. NAS3-21603
		13. Type of Report and Period Covered Contractor Report
12. Sponsoring Agency Name and Address National Aeronautics and Space Administration Lewis Research Center Cleveland, OH.		
		14. Sponsoring Agency Code

15. Supplementary Notes

16. Abstract   An analytical technique for the prediction of fan blade flutter is evaluated by utilizing first-stage fan flutter data available from tests conducted at the National Aeronautics and Space Administration (NASA), Lewis Research Center on an advanced high performance engine. The formulation includes both aerodynamic and mechnical coupling among all the blades of the assembly. Mistuning is accounted for in the analysis so that individual blade inertias, frequencies, or damping can be considered. Airfoil stability is predicted by calculating a flutter determinant, the eigenvalues of which indicate the extent of susceptibility to flutter.

When blade-to-blade differences in frequencies are considered in the analysis a stable system is predicted for the test points examined in this report. For a tuned system, however, it was found that torsional flutter can be predicted at a limited number of interblade phase angles. An examination of these phase angles indicated that they were "close" to the condition of acoustic resonance. For the range of Mach numbers and reduced frequencies considered here, the so-called subcritical flutter cannot be predicted.

The essential influence of mechanical coupling among the blades is to change the frequencies of the system with little or no change in damping. But, aerodynamic coupling together with mechanical coupling could change not only frequencies but also damping in the system, with a trend toward instability.

17. Key Words (Suggested by Author(s)) Subsonic stall flutter Unsteady aerodynamics Aerodynamic Coupling Mechanical coupling Aeroelasticity Mistuning	18. Distribution Statement		
19. Security Classif. (of this report) Unclassified	20. Security Classif. (of this page) Unclassified	21. No. of Pages 54	22. Price*

NASA-C-168 (Rev. 6-71)

FOREWORD

The development of the analysis presented herein was sponsored by the National Aeronautics and Space Administration, Lewis Research Center under Contract NAS3-21603. The NASA Project Manager was Dr. A. P. Kurkov whose assistance in providing the input data and test results for the test cases and development of the computer analysis is gratefully acknowledged.

Principal United Technologies Research Center (UTRC) participants in the contract activity were Dr. A. V. Srinivasan, Dr. S. Sridhar, and Mr. R. LaBarre. Dr. Srinivasan was the Principal Investigator and Program Manager with primary responsibility for the development and application of the analysis and was the author of the Final Report. Dr. Sridhar was responsible for the development of the analysis of the "shroud ring" influence coefficients and Mr. LaBarre was responsible in developing the computer program based on the analyses.

This report is the final documentation of a blade flutter prediction model evaluation performed at UTRC by comparing the analytical predictions with corresponding flutter test data available for a part-span shrouded fan assembly.

LIST OF ILLUSTRATIONS

ii

iii

LIST OF TABLES

TABLE OF CONTENTS

SUMMARY

An analytical technique for the prediction of fan blade flutter is evaluated by utilizing first-stage fan flutter data available from tests conducted at the National Aeronautics and Space Administration (NASA), Lewis Research Center on an advanced high performance engine. The formulation includes both aerodynamic and mechnical coupling among all the blades of the assembly. Mistuning is accounted for in the analysis so that individual blade inertias, frequencies, or damping can be considered. Airfoil stability is predicted by calculating a flutter determinant, the eigenvalues of which indicate the extent of susceptibility to flutter.

When blade-to-blade differences in frequencies are considered in the analysis a stable system is predicted for the test points examined in this report. For a tuned system, however, it was found that torsional flutter can be predicted at a limited number of interblade phase angles. An examination of these phase angles indicated that they were "close" to the condition of acoustic resonance. For the range of Mach numbers and reduced frequencies considered here, the so-called subcritical flutter cannot be predicted.

The essential influence of mechanical coupling among the blades is to change the frequencies of the system with little or no change in damping. But, aerodynamic coupling together with mechanical coupling could change not only frequencies but also damping in the system, with a trend toward instability.

1

INTRODUCTION

An important factor which influences the development program of any advanced engine is the susceptibility of rotor blades to flutter instabilities. In order to understand more fully the mechanism of fan blade flutter instabilities and the parameters that influence flutter, several tests on an advanced engine were conducted at NASA Lewis. These tests covered a wide range of realistic operating conditions appropriate to a modern high performance jet engine. Considerable data were generated for the component under study (i.e., the part-span-shroud fan assembly). Documentation of the steady-state aerodynamic conditions prevailing at the several test points, compilation, and analysis of flutter data may be found in reference 1. Detailed analysis of aerodynamic data obtained from high response pressure probes and optical probes are presented in reference 2.

The nature of flutter observed in all these tests was subsonic stall flutter and a study of the flutter mode of vibration revealed the presence of several harmonics in a nearly pure torsional mode. Frequency measurements made on each blade fully restrained at its shroud revealed blade-to-blade differences. Considerations of all these aspects of the problem pointed to the need to develop an analytical model which can account for blade mistuning in the analysis. This report summarizes the results of a preliminary effort to model the flutter characteristics of a mistuned rotor.

In as much as the observed flutter mode was concluded to be essentially an above shroud first torsional mode, the analytical model represents each blade as a torsional oscillator. The oscillators are assumed to be mounted on a ring representing the shroud. The formulation allows for blade-to-blade differences in any or all of the following: frequency, inertia, damping. The unsteady aerodynamic coefficients used in this study are based on the analysis due to Smith (reference 3). The problem is formulated along the lines outlined by Whitehead (reference 4) and leads to a flutter determinant, the solution of which yields the eigenvalues at which flutter is likely to occur. The real parts of the eigenvalues represent the frequencies at which flutter may occur and the corresponding imaginary parts represent the level of damping.

In this report, the technical approach, along with a discussion of its principal features, is outlined first. The application of the analytical model to four test points is discussed next, followed by a discussion and summary of the results covering the conclusions drawn from the comparisons made between the analytical model and test results. The detailed derivations are shown separately in the APPENDICES.

2

NOMENCLATURE

A   Aeroelastic moment

(A) Matrix of aerodynamic effects

C_M Unsteady aerodynamic moment coefficient

(C) Matrix of C_M

c   Blade chord

E   Modulus of elasticity

(E)   Matrix of interblade phase angles, see Eq. (11) of APPENDIX A

f   Force between blade and support structure

I   Mass moment of inertia of a blade/unit length or moment of inertia of ring cross section

(I) Matrix of blade inertia ratios

K   Blade stiffness

M   Mach number

(M)   Matrix of mechanical effects

n   Nodal diameter (harmonic number)

N   Number of blades

p   Frequency parameter $\left(\dfrac{\omega^2 - \omega_0^2}{\omega_0^2}\right)$

S   Gap between blades

t   Time

u   Aerodynamic modal twist

U   Steady fluid velocity relative to blade

w   Amplitude of vibratory rotation of support structure

y	Amplitude of vibratory rotation of support structure
z	$y-w$
α	Dynamic influence coefficient
β	Interblade phase angle
γ	Individual blade frequency departure parameter
δ	Logarithmic decrement
μ	Ratio of aerodynamic inertia to blade inertia
ν	Frequency parameter $\left(\dfrac{\omega_0^2 - \omega^2}{\omega^2}\right)$
η	Elastic axis position expressed as a percentage of chord from the leading edge
ω	Circular frequency of vibration
λ	Reduced frequency $c\omega/U$
θ	Blade stagger relative to tangential plane
ρ	Air density
ζ	Damping ratio

Subcripts

AR	Acoustic resonance
α	Twist
F	Force
I	Imaginary part
M	Moment
o	Leading edge position (or reference blade)
q	Translation
R	Real part
T	Tangential

4

TECHNICAL APPROACH

Overview

The approach adopted here considers the differential equations of motion governing the vibration of a cascade of blades in a uniform flow field. Thus, the forces acting on each member of the cascade include aerodynamic forces in addition to mechanical (inertial, restoring, and damping) forces. The aerodynamic forces acting on the system not only influence the vibratory motion of the blades but are, in turn, influenced by vibration. These aeroelastic forces are generally dependent on the prevailing steady-state aerodynamic conditions, cascade geometry, and the mode of vibration. For a complete description of the aerodynamic force it is also necessary to know the location of the elastic axis. As each blade is a member of an assembly of blades vibrating in a flow field, the vibration of each member influences every other member and thus all blades are aerodynamically coupled. In addition, the blades can also be coupled mechanically through the disk on which they are mounted or through the shrouds at which each blade comes into contact with its neighbors due to blade untwist at speed.

The above considerations lead to a formulation which describes the motion of a system of blades coupled aerodynamically and mechanically. By virtue of mistuning in which one or more characteristic (frequency, damping, etc.) of each blade is "slightly" different from those of a reference blade, the system of equations leads to a flutter determinant, the solution of which yields the possible frequencies of vibration at which the system is susceptible to flutter.

The construction of the mathematical model proceeded on the basis of representing only the above-shroud-torsion vibration mode of an advanced fan. Thus the analysis is restricted to modeling the blades as linear torsional oscillators supported on a flexible "shroud ring". The validity of the model and the associated computer program was established by making comparisons with appropriate published analytical results. Upon validating the model, several flutter test points were chosen from available data and analyzed to determine if the analytical results indicated trends observed in tests.

Analytical Model Development

The details of the analysis are presented in APPENDIX A. The complex eigenvalues $\{\nu\}$ are sought as a solution to the matrix equation

$$\left(M + \frac{\mu}{\lambda^2} A \right) \{f\} = \nu \{f\} \tag{1}$$

where the matrix $M = \bar{\bar{\alpha}}\, \bar{\jmath} - I$ represents mechanical effects and the matrix $A = (\bar{\bar{\alpha}})(E)(C)(E)^{-1}$ represents the aeromechanical effects; $(\bar{\bar{\alpha}})$ is a matrix whose elements include the dynamic influence coefficients of the support structure; μ represents the inertia ratio; and λ is the reduced frequency. In terms of Whitehead's notation the eigenvalues p are calculated from ν using the simple relationship

$$p = \left(\frac{-\nu}{1 + \nu} \right) \approx -\nu \tag{2}$$

Unless otherwise indicated, the results presented in this report show the values of p rather than ν. The real part of p represents the departure of the frequency of vibration from that of the reference blade (i.e., $\left(p_R = \dfrac{\omega_R^2 - \omega_0^2}{\omega_0^2} \right)$), and the imaginary part of p represents damping in the system in terms of the loss factor. The latter is a commonly used measure of structural damping and is defined as the ratio of specific damping energy to the maximum strain energy per unit volume of the vibrating body.

Some of the principal assumptions inherent in the analysis are worth noting. The dynamic influence coefficients of the "shroud ring" which are derived in APPENDIX B are dependent on the frequency of vibration of the entire system. Thus the ring is characterized at a reference frequency in much the same way the disk was characterized in reference 5. Further, the manner in which λ enters into the analysis is such that the calculations are made for a fixed λ.

The analysis and the associated computer program are developed in such a way that the unsteady aerodynamic coefficients needed in the calculations may be obtained from any available analysis and used as input. However, the results reported here are all based on the use of the complex coefficients calculated by the method given by Smith (reference 3). Smith's analysis is based on the assumption that the blades can be represented by flat plates at

6

zero mean incidence, that the flow is subsonic, isentropic, and two-dimensional and that the Kutta-Joukowski condition at the trailing edge is satisfied.

Calculation Procedure

The unsteady aerodynamic coefficients were first calculated for a given cascade geometry and these were transferred to the appropriate elastic axis position. The extent of mistuning in terms of departure of blade frequency and/or damping and/or blade inertia from those of the corresponding mean values are used as input. To include mechanical coupling among the blades through the supporting "ring", the dynamic influence coefficients appropriate at the reference frequency were calculated and used in computing the matrices M and A. Eigenvalues and eigenvectors were then computed using the method of approach available in the EISPAK package (see reference 6).

For a single degree of freedom representation, a positive sign on the imaginary part of the aerodynamic coefficient implies negative aerodynamic damping and, therefore, for a tuned rotor no further calculations will be needed to determine which of the test points were likely to indicate flutter. The condition for incipient flutter is therefore obtained by setting the imaginary part of the aerodynamic coefficient to zero. i.e.,

$$\left(C_{M_{\alpha_I}}\right)_o - \eta\left(C_{F_{\alpha_I}}\right)_o - \lambda\eta\left(C_{M_{q_R}}\right)_o + \lambda\eta^2\left(C_{F_{q_R}}\right)_o = 0 \tag{3}$$

A solution of this quadratic in η provides the positions of the elastic axis appropriate for flutter to occur for prescribed values of λ and β. However, when mistuning is included, a complete solution of the flutter determinant is necessary so that only the nature of the complex eigenvalues for the system can determine the extent of flutter.

Analytical Model Verification

A series of results was generated for a twelve-bladed system in order to validate the accuracy of the computer program and to illustrate the various features of an aeromechanically coupled assembly of vibrating blades. Figure 1 illustrates the eigenvalues for the undamped and tuned blades supported on a flexible ring. Only mechanical coupling effects are shown in figure 1. As the support structure does not distinguish between forward and backward traveling waves, only six (N/2) distinct eigenvalues are calculated. The ring was characterized at a reference frequency (f_o = 1098 cps). As expected, some of the eigenvalues for the mechanically coupled system are higher than those of the reference frequency and some lower. The extent of departure depends entirely on the proximity of the ring eigenvalues to the frequency at which the ring is characterized.

On the other hand, if the same system is coupled through aerodynamics, the eigenvalues are unsymmetrically distorted as shown in figure 2 and result in a locus, the real part of which represents the frequencies of vibration of the system and the imaginary part represents the damping. The asymmetry (i.e., the frequencies of the forward and backward traveling waves being somewhat different from each other) is due to the dependence of the aerodynamic coupling forces on the direction of the wave (i.e., the sign of the interblade phase angle).

The results of mistuning alternate blades is shown in figure 3. Figure 3 also illustrates the manner in which the locus of the eigenvalues shifts with (a) the addition of mechanical damping, and (b) the removal of all aerodynamic coupling. From figure 3 it is clear that the locus of eigenvalues shifted upward (toward more stable condition) indicating a correct trend. Further, with the removal of all aerodynamic coupling, the locus reduces to clusters of points. The magnitude of the imaginary part of the eigenvalue (i.e., 0.0044) is δ/π so that $\delta = 0.0137$ which agrees with the logarithmic decrement input.

The cascade parameters used to generate the loci of figure 2 are the same as those of reference 4. The unsteady aerodynamic coefficients were calculated for interblade phase angles $\beta = 2\pi n/N$ from n=1 to N. The departure of each blade frequency from the mean (γ) and the damping distribution (δ) were obtained by enlarging figure 18 of reference 4 and picking out the numbers from the enlarged figure (see TABLE I). These were then used in calculating the effects of mistuning and the results are shown in figure 2. The eigenvector corresponding to the least stable eigenvalue is shown in figure 4. The lack of correlation at one point in figure 2 is attributed to the fact that $\beta=0$ (or 2π) is specifically excluded in the computer program used to calculate the unsteady coefficients. The combination $M=0, \beta=0$ is of little interest in practice and therefore no further studies were made. The strength of each harmonic present in a mistuned mode is calculated as a part of the computer program as shown in figure 5. As observed by Whitehead in reference 4, the eigenvector has a predominantly two nodal diameter pattern, as can be seen from figure 5.

Figure 6 shows the effects of both aerodynamic and mechanical coupling on the locus of eigenvalues. Due to the addition of mechanical coupling, the locus of eigenvalues does not shift uniformly and the frequencies corresponding to an interblade phase angle may increase, decrease, or experience little or no change at all. Comparison of figures 6 and 1 indicates the nature of frequency shifts shown in figure 6 corresponds closely to those shown in figure 1. Thus, the eigenvalues corresponding to nodal diameter patterns ± 3 and ± 4 in figure 6 are affected most and in a manner similar to that shown in figure 1. The mechanical coupling corresponding to figure 6 was obtained for a

8

stiff and "oversized shroud ring". A more realistic case corresponding to a more flexible coupling among the blades will be considered later in connection with the analysis of a 38 bladed rotor.

Reference to figure 7 confirms the nature of the eigenvectors typical of a mistuned system. The waviness present in the phase angle confirms the nonconstant nature of the interblade phase angle; an important feature of a mistuned system. Further, an eigenvector corresponding to an eigenvalue for a mistuned system contains in it contributions from several modes of the tuned system.

Mechanical Coupling Among Blades

Since the vibration modeling is restricted to considerations of above-shroud torsional mode only, the shroud is assumed to serve as a support for the blades. Thus the deformation of the shroud couples all the blades. The shroud is modeled as a continuous ring whose dynamic influence efficients were calculated at a frequency of 1098 Hz; this frequency being the average of the 38 blade frequencies. The latter were obtained from reference 1. The influence coefficients exhibited the expected characteristics which included (a) identical numbers on the principal diagonal, (b) complete symmetry, and (c) identical numbers on each subdiagonal. For a 38 bladed rotor, calculations were made using the actual dimensions of the "shroud ring" supported by springs in a plane perpendicular to that of the ring. The stiffness of the springs (139.931 N/m/radian) was obtained from an available NASTRAN run for the zeroth harmonic of the fan assembly.

APPLICATION OF ANALYTICAL MODEL

The test points at which flutter was observed in the advanced fan are marked on the fan map shown in figure 8. The analysis procedure and the associated computer program were applied to calculate the susceptibility to flutter for four test points (i.e., Nos. 118, 123, 125, and 127). The steady-state aerodynamic conditions for these test points are fully documented in reference 1. The first step was to calculate the unsteady aerodynamic coefficients for each of these points for a representative section of the blade and examine their behavior. The tip section was chosen as the representative section in this study.

Figure 9 shows the loci of the aerodynamic coefficients. An examination of the coefficients for points 118 and 125 shows the extent of sensitivity of the unsteady aerodynamic coefficients to the parameters λ and M. Although the difference in λ and M between these test points is only 0.01 and 0.002, respectively, test point 125 indicates flutter ($C_I > 0$) whereas test point 118 does not. While computing these coefficients it was noted that their magnitude varied somewhat with the number of collocation points used on the airfoil. An initial study of this was made for test point 125 using four collocation points (instead of five used in all other calculations) and the results are shown in figure 10. It is noted that even for four collocation points, the results are within experimental accuracy.

At the Mach numbers ($M \approx 0.8$) and reduced frequencies ($\lambda \approx 1.8$), it was noted that the aerodynamic coefficients formed a nearly continuous curve except for a few (three in the cases of test points 118 and 125, for example) coefficients which appeared separate and distinct from the rest. The interblade phase angles corresponding to these particular coefficients were checked to see if they are "close" to either β^S satisfying the acoustic resonance condition. The latter is discussed in some detail in reference 7 and the interblade phase angles can be calculated from the "cut-off" condition to be

$$\beta_{AR} = \frac{S}{C} \left(\frac{\lambda M}{1 - M^2} \right) \left(M \sin \theta \pm \sqrt{1 - M^2 \cos^2 \theta} \right) \tag{4}$$

The regions of flutter in the (η, β) domain are obtained by solving Eq. (4) and are shown in figure 11 for certain cascade conditions which include those of test point 125. Values of β calculated from Eq. (4) are also shown in figure 11. It is clear that under the assumptions discussed earlier, the nature of flutter implied for the test conditions of points 118 and 125 is acoustic resonance. As can be seen from figure 11, this phenomenon occurs over an extremely narrow region of interblade phase angles corresponding to backward traveling waves. The physical significance of this phenomenon in the case of a real machine is not clear.

10

Individual blade frequencies were available for the fan assembly under study and these had been measured (reference 1) with each blade fully restrained at the shroud. The nature of variation of these frequencies is shown in figure 12. Using these frequencies, the mistuned system was analyzed first with aerodynamic coupling only and the results are shown in figure 13. While these results show the system to have positive aerodynamic damping, it is essential to bear in mind that (1) the aerodynamic coefficients are very sensitive to changes in λ and M, as can be seen from a comparison of the coefficients for test points 118 and 125 (see figure 9), and (2) a mistuned mode consists of many interblade phase angles. Thus it is likely that with slight changes in the magnitudes of important parameters, some of the interblade phase angles coincide with those calculated earlier in the acoustic resonance condition.

For the eigenvalue corresponding to the lowest aerodynamic damping in figure 13, the mode shape was calculated and is shown in figure 14. The features of this mode are similar to those of the twelve-bladed system shown in figure 7 and include nonconstant interblade phase angle around the rotor. The mixture of "tuned modes" in the eigenvector calculated at the least positive eigenvalue is clear from figure 15. These calculations show predominant backward traveling waves of nodal diameter patterns 5 and 6 in contrast to a mixture of several forward and backward harmonics Kurkov (reference 8) obtained via analysis of optical displacement data recorded during flutter (see figure 16).

Figure 17 shows the effect of including aerodynamic and mechanical coupling on the eigenvalues of the system. In obtaining these results the "shroud ring" was modeled by using the actual dimensions of the shroud. Two features of these results are worth noting: (1) the lowest aerodynamic damping level dropped from 0.0196 (see figure 13) to 0.0056 upon including mechanical coupling; and (2) the frequency at which damping is the lowest changed from 1175 Hz (7 percent higher than the average blade frequency) to 994 Hz (9.5 percent lower than the average blade frequency).

The mode shape corresponding to the lowest value of aerodynamic damping in figure 17 is shown in figure 18. The strength of several harmonics present in the mode is shown in figure 19. Clearly, a five nodal diameter backward traveling wave is the predominant component.

It may be noted that the position of the elastic axis ($\eta = 0.44$) was chosen on the basis of optical displacement data obtained during flutter. Reference 8 discusses the details of the method used. In order to determine the sensitivity of the aerodynamic coefficients to small changes in η, it was decided to calculate the coefficients for M = 0.795, $\lambda = 1.79$, and $\eta = 0.40$ and compare these with the locus obtained for conditions prescribed for test point 125 (see figure 20).

DISCUSSION OF RESULTS

Among all the factors that enter into the calculation of aerodynamic damping, the most significant is the aerodynamic theory from which the unsteady forces acting on the blade are calculated. The theory chosen for use in this study is based on assumptions of a flat plate cascade and no loading effects are included.

It would be appropriate to repeat these calculations with alternate aerodynamic coefficients. For a given cascade geometry the calculations were found to be very sensitive to changes in Mach number and reduced frequency but less so to inertia ratio. The reduced frequency and Mach number vary from root to tip but considerations of a single representative section such as the tip section does not take into account these variations. Needless to say, a realistic solution should consider modeling the entire blade from root to tip. However, with mistuning included, the problem size can be large unless aerodynamic modal representations are used, in much the same way structural dynamic modal representations are made by use of generalized mass/ inertia and stiffness.

The importance of the phenomenon of acoustic resonance arises from the implication that at the interblade phase angles satisfying Eq. (4), the waves carry energy in a purely tangential direction. The prediction of this type of flutter for the fan considered here is similar to that made in reference 7. The range of interblade phase angles at which acoustic resonance flutter can occur is very narrow and may not correspond to any of the discrete phase angles calculated for a finite number of blades in a cascade. However, as the unsteady pressures acting on blades include a variety of harmonics which are not necessarily integral multiples of the first harmonic, only a detailed analysis of pressure data can answer the question of the relevance of acoustic resonance phenomenon to fan blade flutter.

Mechanical coupling among the blades could change both the real and imaginary parts of the eigenvalues. The extent of such change appears to depend upon the level of stiffness of the support as can be seen from a comparison of figures 6, 13, and 17. The dimensions of the ring used in obtaining the results shown in figure 17 lead to a much more flexible ring than the one used in obtaining the results shown in figure 6. The model used in this report characterizes the "shroud ring" at any one frequency and this was chosen to be the average of all blade frequencies. A drop in frequency of nearly 10 percent from the average suggests a support somewhat more flexible than is present in the real structure as the observed flutter frequency was in the vicinity of 1078 Hz, a mere 2 percent below the average. While the size of the ring cross section could be adjusted to obtain a

12

smaller drop in frequency, it was thought that other assumptions in the analysis should be studied more thoroughly before any revision of the shroud model is considered.

The analytical model developed here considers only one degree of freedom for the blade motion and thus ignores any coupling that may be present among the vibratory modes. Recently Bendicksen and Friedman (reference 9) reported that the influence of coupling on blade flutter calculations is significant. For assemblies which have closely spaced modes, it appears that the inclusion of coupling among the modes of a blade is an appropriate next step in the development of a flutter prediction system.

SUMMARY OF RESULTS

For the cascade conditions appropriate to the test points studied in this report, the aerodynamic theory that was used cannot predict subcritical flutter. Under the assumptions of a tuned assembly, the imaginary part of the aerodynamic coefficients does indicate flutter for a limited number of inter-blade phase angles, but these interblade phase angles are "close" to those at which the so-called acoustic resonance is predicted. Upon using the individual blade frequencies and solving the mistuned system with aerodynamic coupling only, the results show a stable system. Eigenvectors calculated for the mistuned system showed the presence of several harmonics in each mistuned mode. Inclusion of both mechanical and aerodynamic coupling, in the solution of the eigen problem, influences not only the frequencies but also damping in the system with a trend toward instability.

REFERENCES

1. Jeffers, J. D., A. May, and W. J. Deskin: Evaluation of a Technique for Predicting Stall Flutter in Turbine Engine. NASA CR 135423, 1978.

2. Kurkov, A. P. and H. H. Dicus: Synthesis of Blade Flutter Vibratory Patterns Using Stationary Transducers. ASME Paper 78-GT-160.

3. Smith, S. N.: Discrete Frequency Sound Generation in Axial Flow Turbomachines. R&M 3709, 1971.

4. Whitehead, D. S.: Torsional Flutter of Unstalled Cascade Blades at Zero Deflection. R&M 3429, 1964.

5. El-Bayoumy, L. E. and A. V. Srinivasan: Influence of Mistuning on Rotor-Blade Vibrations. AIAA J., Vol. 13, No. 4, April 1976, pp 460-464.

6. Smith, B. T., et al.: Lecture Notes in Computer Science. Springer-Verlag, 1974.

7. Whitehead, D. S.: The Effect of Compressibility on Unstalled Torsional Flutter. CUED/A-Turbo/TR51, Aug. 1973.

8. Kurkov, A. P.: Flutter Spectral Measurements Using Stationary Pressure Transducers. Measurements Methods in Rotating Components of Turbomachinery, ASME, N.Y., 1980.

9. Bendicksen, O. and P. Friedman: Coupled Bending-Torsion Flutter in Cascades. AIAA Paper 79-07983, Presented at the 20th Structures, Structural Dynamics, and Materials Conference, April 1979.

APPENDIX A: FORMULATION OF ANALYTICAL MODEL

Governing Equations of Motion

The vibration of kth blade is given by

$$I_k \ddot{y}_k - A_k + c_k \dot{z}_k + K_k z_k = 0 \tag{1}$$

where

$$z_k = y_k - w_k \tag{2}$$

Let

$$f_k = c_k \dot{z}_k + K_k z_k \tag{3}$$

where I_k = Mass moment of inertia of kth blade blade/unit length

K_k = k^{th} blade stiffness

c_k = Mechanical damping associated with k^{th} blade

y_k = amplitude of vibratory motion of kth blade

w_k = amplitude of vibratory motion of support structure at k^{th} blade

A_k = aeroelastic forces acting on k^{th} blade.

The vibratory motion around the support structure (shroud "ring" or disk) at any blade location may be written as

$$w_k = \sum_{\ell=1}^{N} \alpha_{k\ell}^{s} f_{\ell} \tag{4}$$

Where $\alpha_{k\ell}^{s}$ represents the vibratory motion of the support structure at k due to a unit stimulus at ℓ.

Clearly, $\alpha_{k\ell} = \alpha_{k\ell}(\omega)$, where ω is the frequency (of the forcing function) and N is the total number of blades.

$$f_k = c_k \overline{(\dot{y}_k - w_k)} + K_k (y_k - w_k) \tag{5}$$

16

$$y_k = \sum \alpha_{k\ell}{}^s f_\ell + \alpha_{kk}{}^b \qquad (6)$$

and with $y = \hat{y}\, e^{i\omega t}$, $y_k - w_k = \alpha_{kk}{}^b f_k$ where the superscript b refers to blade
Thus,

$$y_k = \sum \alpha_{k\ell}\, f_\ell \qquad (7)$$

where

$$\alpha_{k\ell} = \alpha_{k\ell}^s + \alpha_{kk}^b$$

Equation (1) may then be rewritten as

$$-\omega^2 (\mathcal{J})(\alpha)\{f\} - \{A\} + \{f\} = 0 \qquad (8)$$

where ($\mathcal{J}$) is the inertia matrix

(α) is the matrix of dynamic influence coefficients of the support
   structure and blade

$\{A\}$ is a column matrix representing the aeroelastic moments.

Aeroelastic Moments

Let u_r represent y_k in the rth mode. The total amplitude of the kth blade
is the sum of all complex amplitudes from all contributing modes.

$$\text{i.e.} \quad y_k = \sum_{r=1}^{N} u_r e^{ik\beta_r} \qquad (9)$$

Where β_r is the interblade phase angle corresponding to the rth mode
(i.e., $\beta_r = \dfrac{2\pi r}{N} = r\beta_1$ and $k\beta_r = r\beta_k$). Thus,

$$\{y\} = (E)\{u\} \qquad (10)$$

where (E) represents the matrix consisting of interblade pahse angles, i.e.,

$$
(E) = \begin{pmatrix} e^{i\beta_1} & e^{i2\beta_1} \dots e^{iN\beta_1} \\ e^{i2\beta_1} & e^{i4\beta_1} \\ e^{iN\beta_1} & e^{iN^2\beta_1} \end{pmatrix} \tag{11}
$$

The aeroelastic moment acting on the kth blade, due to motion in the rth mode alone can be written as

$$
A_{k_r} = \pi \rho U^2 c^2 C_{M_r} u_r e^{ik\beta_r} e^{i\omega t} \tag{12}
$$

where ρ is the air density

   U is the air velocity

   c is blade chord

   C_{M_r} is the unsteady aerodynamic moment coefficient corresponding to a cascade of blades oscillating in the rth mode.

Let η represent the elastic axis position expressed as a percentage of chord measured from the leading edge of the airfoil. Then,

$$
C_M = (C_{M\alpha})_\eta = (C_{M\alpha})_0 - \eta (C_{F\alpha})_0 - i\lambda\eta(C_{Mq})_0 + i\lambda\eta^2 (C_{Fq})_0 \tag{13}
$$

where C_{m_α} represents the moment coefficient with $\eta = 0$.

C_{F_α}, C_{F_q} represents the unsteady aerodynamic force coefficients due to vibratory twist α and displacement q, respectively.

The total contribution to the aeroelastic moment acting on the kth blade, from all modes can be written as

$$
\{A\} = \pi \rho U^2 c^2 e^{i\omega t} (E)(C)(E^{-1})(\alpha)\{f\} \tag{14}
$$

Therefore, the governing equations of motion in terms of the force $\{f\}$ transmitted to the supporting structure may be written as

$$
\left[-\omega^2 (\mathcal{I})(\alpha) + \pi \rho U^2 c^2 (E)(C)(E)^{-1}(\alpha) + I \right] \{f\} = \{0\} \tag{15}
$$

18

The kth element of (α) may be shown to be

$$\frac{1 + \alpha_{kk}^s \frac{\mathcal{I}_k}{\mathcal{I}_0} \frac{\omega_k^2}{\omega_0^2} \mathcal{I}_0 \omega_0^2 \left\{ 1 + 2i \frac{\omega}{\omega_0} \frac{\omega_0}{\omega_k} \frac{\zeta_k}{\zeta_0} \zeta_0 \right\}}{\mathcal{I}_0 \omega_0^2 \frac{\mathcal{I}_k}{\mathcal{I}_0} \frac{\omega_k^2}{\omega_0^2} \left(1 + 2i \frac{\omega}{\omega_0} \frac{\omega_0}{\omega_k} \frac{\zeta_k}{\zeta_0} \zeta_0 \right)} \qquad (16)$$

where $\mathcal{I}_0$ and ω_0 refer to the inertia and frequency of the reference blade. The k_j^{th} element of (α) is simply α_{kj}^s

The governing Eq. (15) can then be rewritten as

$$\left[-\omega^2 \mathcal{I}_0 (\bar{\mathcal{I}})(\bar{\alpha}) - \frac{\pi \rho c^4 \omega^2}{\lambda^2} (E)(C)(E^{-1})(\alpha) + I \right] \{f\} = \{0\} \cdots \qquad (17)$$

$$\left(\lambda = \frac{\omega c}{U} \right)$$

The elements of $\bar{\alpha}$ are as shown in Eq. (16) and $(\mathcal{I}) = (\mathcal{I}_1/\mathcal{I}_0, \mathcal{I}_2/\mathcal{I}_0 \cdots \mathcal{I}_N/\mathcal{I}_0)$

$$\left[-(\bar{\mathcal{I}})(\bar{\alpha}) - \frac{\mu}{\lambda^2} (E)(C)(E)^{-1}(\bar{\alpha}) + I \right] \{f\} = \{0\} \qquad (18)$$

The elements of $\bar{\bar{\alpha}}$ are those shown in Eq. (16) multiplied by $\mathcal{I}_0 \omega^2$ and $\mu = \frac{\pi \rho c^4}{I_0}$ representing the ratio of aerodynamic inertia to blade inertia.

For the sake of clarity, the elements of $\bar{\bar{\alpha}}$ are shown below.

$$\bar{\bar{\alpha}}_{kk} = \frac{\omega^2}{\omega_0^2} \frac{1 + \alpha_{kk}^s \mathcal{I}_0 \omega_0^2 \mathcal{I}_k \omega_R^2 \left(1 + 2i \frac{\omega}{\omega_0} \frac{1}{\omega_R} \zeta_R \zeta_0 \right)}{\mathcal{I}_R \omega_R^2 \left(1 + 2i \zeta_0 \frac{\omega}{\omega_0} \frac{1}{\omega_R} \zeta_R \right)} \qquad (19)$$

$$\bar{\bar{\alpha}}_{kj} = \mathcal{I}_0 \omega_0^2 \frac{\omega^2}{\omega_0} \alpha_{kj}^s$$

$\mathcal{I}_r$, ω_r, etc. represent the ratio of blade inertia and frequency etc. (i.e., inertia of blade/inertia of reference blade, frequency of blade/frequency of reference blade, etc.). Multiplying throughout by ω_0^2/ω^2, Eq. (19) can be written as

$$\left[(-\bar{\mathcal{I}})(\bar{\bar{\alpha}}) - \frac{\mu}{\lambda^2} (E)(C)(E)^{-1}(\bar{\bar{\alpha}}) + \frac{\omega_0^2}{\omega^2} (I) \right] \{f\} = \{0\} \cdots \qquad (20)$$

19

Clearly, the elements of $\bar{\bar{\alpha}}$ are the same as those shown in Eq. (19) except for the quantity ω^2/ω_o^2 which is divided out. Let $\omega_o^2/\omega^2 = (1+\nu)$ and Let $M = (\bar{\bar{\alpha}})(\mathcal{J}) - I$ represent mechanical coupling effects, and $\langle A \rangle = \mu/\lambda^2 \bar{\bar{\alpha}}(E)(C)(E^{-1})$ represent aeromechanical coupling effect. Then Eq. (20) can be shown to reduce to

$$\left(M + \frac{\mu}{\lambda^2} A \right) \{f\} = \nu\{f\} \tag{21}$$

Equation (21) represents the required eigenvalue formulation.

Clearly, the solution ν provides the frequencies (real part) and damping (imaginary) at these frequencies. If p is defined in accordance with Whitehead's notation, as

$$p = \frac{\omega^2 - \omega_o^2}{\omega_o^2}, \text{ then } p = \frac{-\nu}{1+\nu} \approx -\nu$$

20

APPENDIX B: DYNAMIC INFLUENCE COEFFICIENTS FOR "SHROUD RING"

The shrouds on the blades are assumed to form a continuous ring. The derivation of the dynamic influence coefficients is based on the following assumptions:

1. The ring is circular, homogeneous, and isotropic.

2. The ring is supported on an elastic foundation.

3. Only out-of-plane small (linear) vibrations are considered.

4. Effect of rotary inertia is included.

5. Effect of shear deformation is neglected.

The shroud ring model and the forces and moments acting on an element of the ring are shown in figure 22. Referring to figure 22, and assuming that the elemental angle $d\theta$ is small, the force and moment equilibrium equations can be written as

$$\frac{\partial V}{\partial \theta} = kw - f + m \frac{\partial^2 w}{\partial t^2} \ , \tag{1a}$$

$$\frac{\partial M_T}{\partial \theta} + M_B = 0 \ , \tag{1b}$$

$$\frac{\partial M_B}{\partial \theta} - M_T + RV - F = \frac{mr^2}{R} \frac{\partial^2}{\partial t^2} \left(\frac{\partial w}{\partial \theta} \right) \tag{1c}$$

Here, $w(\theta, t)$ is the deflection, V is the shear force, M_T is the torsional moment, M_B is the bending moment, m is the mass per radian, k is the stiffness per radian of the support, R is the radius of the ring, r is the radius of gyration of the cross section of the ring, f is the external force per radian, and F is the external moment per radian. The governing equation of motion is obtained by differentiating Eq. (1c) with respect to θ, using Eqs. (1a) and (1b), and noting that

$$M_B = \frac{EI}{R^2} \frac{\partial^2 w}{\partial \theta^2}$$

21

The equation of motion is

$$\frac{EI}{R^2}\left(\frac{\partial^4 w}{\partial\theta^4} + \frac{\partial^2 w}{\partial\theta^2}\right) + Rkw + Rm\frac{\partial^2 w}{\partial t^2} - \frac{mr^2}{R}\frac{\partial^4 w}{\partial\theta^2\partial t^2} = Rf + \frac{\partial F}{\partial\theta} \qquad (2)$$

The appropriate boundary conditions are:

1. $w(0,t) = w(2\pi,t)$; $\dfrac{\partial^n w}{\partial\theta^n}(0,t) = \dfrac{\partial^n w}{\partial\theta^n}(2\pi,t)$ $\qquad$ (3a)

2. For a single external force, $f_k d\theta$, acting alone at $\theta = \theta_k$,

$$\frac{\partial w}{\partial\theta}(\theta_k,t) = 0 \qquad (3b)$$

3. For a single external moment, $F_k d\theta$, acting alone at $\theta = \theta_k$,

$$w(\theta_k,t) = 0 \qquad (3c)$$

Free Vibrations

The problem of free vibrations is obtained by setting $f \equiv 0$ and $F \equiv 0$ in Eq. (2). The solution which satisfies the boundary condition, Eq. (3a), can be written as

$$w(\theta,t) = \phi_n(\theta)e^{i\lambda_n t} \qquad (4)$$

where

$$\phi_n = a_n \cos n\theta \qquad (5)$$

$$\lambda_n^2 = \frac{1}{mR(R^2 + n^2 r^2)}\left[EIn^2(n^2-1) + kR^3\right], \quad n = 0,1,2,\dots, \qquad (6)$$

and $\theta = \theta$ is arbitrary. The coefficients, a_n, in Eq. (5) are chosen such that

$$\int_0^{2\pi} \phi_n M\left[\phi_n\right]d\theta = 1; \quad M \equiv \frac{m}{R}\left(R^2 - r^2\frac{d^2}{d\theta^2}\right)$$

so that,

$$a_0 = (2\pi m R)^{-\frac{1}{2}} \qquad\qquad \text{, for } n=0, \tag{7a}$$

$$a_n = \left[\frac{\pi m}{R}(R^2 + n^2 r^2)\right]^{-\frac{1}{2}} \qquad\qquad \text{, for } n \geq 1. \tag{7b}$$

Forced Vibrations

In view of the boundary conditions, Eqs. (3b) and (3c), the solution of the forced vibration problem is written as

$$w = w_f + w_F \tag{8}$$

where w_f is the solution for the case of no external moments (i.e., $F \equiv 0$) and w_F is the solution for the case of no external forces (i.e., $f \equiv 0$).

For the case of $F \equiv 0$, the solution can be written as

$$w_f = \sum_n \phi_n^{(k)}(\theta)\, \eta_n(t), \tag{9}$$

where,

$$\phi_n^{(k)} = a_n \cos n(\theta - \theta_k). \tag{10}$$

It is noted that the assumed solution satisfies the boundary condition, Eq. (3b).

By substituting Eq. (9) into Eq. (2), multiplying by $\phi_m^{(k)}$, and integrating from $\theta=0$ to $\theta=2\pi$, one obtains

$$\ddot{\eta}_n + \lambda_n^2 \,\eta_n = R \int_0^{2\pi} f\, \phi_n^{(k)}\, d\theta. \tag{11}$$

The external excitation is assumed to be harmonic, so that,

$$f = \hat{f}\, e^{i\omega t}, \tag{12}$$

where ω is the excitation frequency, and $\hat{f}$ is, in general, complex.

Further, assuming that ω is not equal to λ_n, the solution to Eq. (11) is written as

$$\eta_n = A_n e^{i\omega t} \tag{13}$$

By using Eqs. (9), (11), (12), and (13), one obtains

$$w_f = \left[R \sum_n \phi_n^{(k)} C_n \int_0^{2\pi} \phi_n^{(k)} \hat{f} \, d\theta \right] e^{i\omega t} \tag{14}$$

where,

$$C_n = (\lambda_n^2 - \omega^2)^{-1} \tag{15}$$

Following a procedure similar to the one described above, the solution for the case of $f \equiv 0$ can be obtained as

$$w_F = \left[\sum_n \psi_n^{(k)} C_n \int_0^{2\pi} \psi_n^{(k)} \frac{\partial \hat{F}}{\partial \theta} \, d\theta \right] e^{i\omega t} \tag{16}$$

where,

$$\psi_n^{(k)} = -a_n \sin n(\theta - \theta_k) , \tag{17}$$

and $\hat{F}$ which is, in general, complex is defined by

$$F = \hat{F} e^{i\omega t} . \tag{18}$$

It is noted that Eq. (17) satisfies the boundary condition, Eq. (3c).

The solution of the forced vibration problem, Eq. (8), can be written as

$$w(\theta, t) = \hat{w}(\theta) e^{i\omega t} \tag{19}$$

where,

$$\hat{w} = R \sum_n \phi_n^{(k)} C_n \int_0^{2\pi} \phi_n^{(k)} \hat{f} \, d\theta + \sum_n \psi_n^{(k)} C_n \int_0^{2\pi} \frac{\partial \hat{F}}{\partial \theta} \psi_n^{(k)} \, d\theta . \tag{20}$$

Differentiation of Eq. (19) leads to an expression for the slope, defined by

$$\beta(\theta, t) = \frac{\partial w}{\partial s} = \frac{1}{R} \frac{\partial w}{\partial \theta} \tag{21}$$

24

where,

$$\beta(\theta, t) = \hat{\beta}(\theta) e^{i\omega t} \qquad (22)$$

and

$$\hat{\beta} = \sum_n \frac{d\phi_n^{(k)}}{d\theta} C_n \int_0^{2\pi} \phi_n^{(k)} \hat{f} \, d\theta + \frac{1}{R} \sum_n \frac{d\psi_n^{(k)}}{d\theta} C_n \int_0^{2\pi} \psi_n^{(k)} \frac{\partial \hat{F}}{\partial \theta} \, d\theta \qquad (23)$$

Discretization

To obtain the dynamic influence coefficients for use in the matrix formulation of the mistuning problem, the solutions for the deflection and slope of the shroud ring have to be discretized.

Let, N be the number of blades, k, m, or j the blade number, n the mode number, $\theta = 0$ be fixed at blade number k=1, and $\Delta\theta = (2\pi/N)$. The discretized version of Eq. (20) can be written as

$$\hat{w}_m = R \sum_{n=1}^{N} \phi_{mn}^{(k)} C_{nn} \sum_{j=1}^{N} \phi_{jn}^{(k)} \hat{f}_j \, \Delta\theta + \sum_{n=1}^{N} \psi_{mn}^{(k)} C_{nn} \sum_{j=1}^{N} \psi_{jn}^{(k)} \left(\frac{\partial \hat{F}}{\partial \theta}\right)_j \Delta\theta \qquad (24)$$

where,

$$C_{nn} \equiv C_n \, ,$$

$$\phi_{mn}^{(k)} = a_n \cos n (\theta_m - \theta_k), \qquad (25a)$$

$$\psi_{mn}^{(k)} = - a_n \sin n (\theta_m - \theta_k), \qquad (25b)$$

for n=0, 1, 2... and m, k=1, 2, 3...

Letting,

$$\left(\frac{\partial \hat{F}}{\partial \theta}\right)_j = \frac{1}{2\Delta\theta} \, (\hat{F}_{j+1} - \hat{F}_{j-1}) \quad ,$$

$$q_m = \hat{f}_m \Delta\theta, \, Q_m = \hat{F}_m \Delta\theta$$

in Eq. (24), and after some algebra, the matrix version of Eq. (24) can be written as

25

$$\{\hat{w}\} = \left[\alpha^1\right]\{q\} + \left[\alpha^2\right]\{Q\} \tag{26}$$

where $\hat{w}$, q, and Q are N-vectors, and α^1, α^2 are NxN matrices, whose elements are given by

$$\alpha^1_{mk} = R \sum_{n=0}^{N} \phi_{mn}^{(k)} C_{nn} a_n \tag{27a}$$

$$\alpha^2_{mk} = \frac{N}{4\pi} \sum_{n=0}^{N} \psi_{mn}^{(k)} C_{nn} \sum_{j=1}^{N} \psi_{jn}^{(k)} E_{jk} \quad , \tag{27b}$$

m refers to the row, k refers to the column, and

$$[E] = \begin{bmatrix} 0 & 1 & 0 & & 0 & -1 \\ -1 & 0 & 1 & & & 0 \\ 0 & -1 & 0 & 1 & & \\ & & -1 & 0 & 1 & 0 \\ 0 & & & -1 & 0 & 1 \\ 1 & 0 & & 0 & -1 & 0 \end{bmatrix} \tag{28}$$

Following a procedure similar to the one described above, the matrix version of Eq. (23) can be written as,

$$\{\beta\} = \left[\alpha^3\right]\{q\} + \left[\alpha^4\right]\{Q\} \tag{29}$$

where,

$$\alpha^3_{mk} = \sum_{n=0}^{N} n \, \psi_{mn}^{(k)} C_{nn} a_n \tag{30a}$$

$$\alpha^4_{mk} = - \frac{N}{4\pi R} \sum_{n=0}^{N} n \, \phi_{mn}^{(k)} C_{nn} \sum_{j=1}^{N} \psi_{jn}^{(k)} E_{jk} \quad . \tag{30b}$$

Equations (26) and (29) can be combined to give the dynamic influence coefficient matrix as,

$$\begin{bmatrix} \left[\alpha^1\right] & \left[\alpha^2\right] \\ \left[\alpha^3\right] & \left[\alpha^4\right] \end{bmatrix}$$

TABLE I

DEPARTURES OF INDIVIDUAL BLADE FREQUENCIES (γ) AND
DISTRIBUTION OF DAMPING (δ) USED IN MODEL VERIFICATION
Reference 4, figure 18

k	γ_k	δ_k/π
1	0	0.0025
2	-0.0055	0.0040
3	-0.0015	0.0020
4	-0.0008	0.0026
5	0	0.0025
6	0.0013	0.0022
7	0.0010	0.0029
8	0.0002	0.0052
9	0.0002	0.0052
10	0	0.0056
11	0.0019	0.0055
12	0.0034	0.0055

Figure 1 Eigenvalues for a 12 Bladed Tuned System (Mechanical Coupling Only)

□ NUMBERS INDICATE NODAL DIAMETER PATTERNS

$(EI)_{RING} = 8863.7$ Nm^2

DATUM FREQUENCY = 1098 cps (f_o)

RING FREQUENCY (CPS) = 0.000, 391.6, 954.0, 1728.8, 2707.8, 3879.8, 5232.0, 6750.7,
8421.3, 10229.4, 12160.7, 14201.2

$$p = \frac{(\omega^2 - \omega_o^2)}{\omega_o^2}$$

REAL PART OF p

IMAGINARY PART OF p

.005 0 -.005 -.010 -.015

0.2 0 -0.2 -0.20

±4 ±5 ±1±6 ±2 ±3
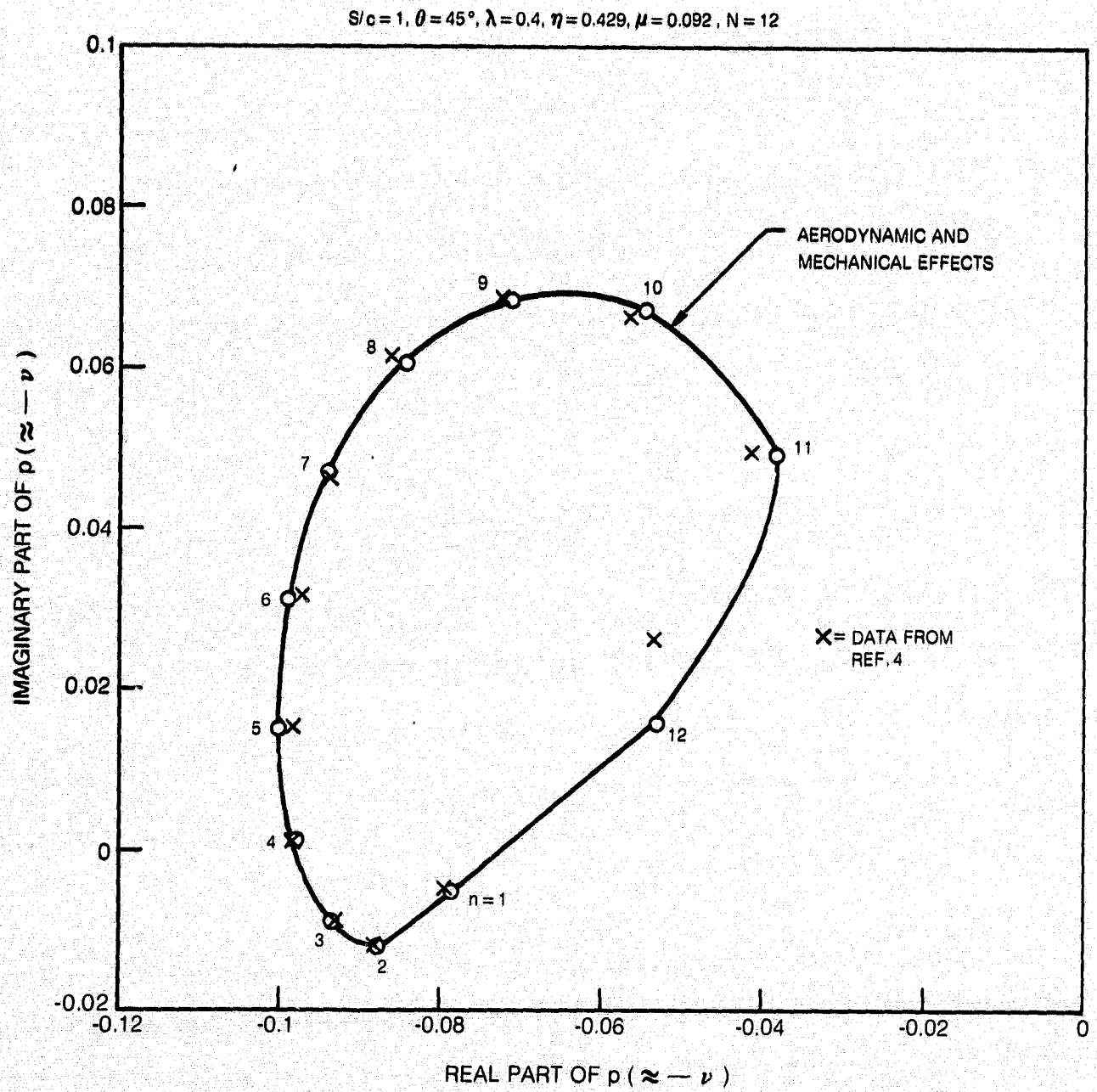
Figure 2 Effect of Mistuning on Eigenvalues

(ALTERNATE BLADES MISTUNED γ=0.04)

MACH NO. = 0
GAP/CHORD = 1
MASS RATIO = 0.092
η = 0.429
STAGGER = 45°
λ = 0.4
NO. OF BLADES = 12

δ = 0.0137

δ = 0

NO AERODYNAMIC COUPLING

REAL PART OF p

IMAGINARY PART OF p
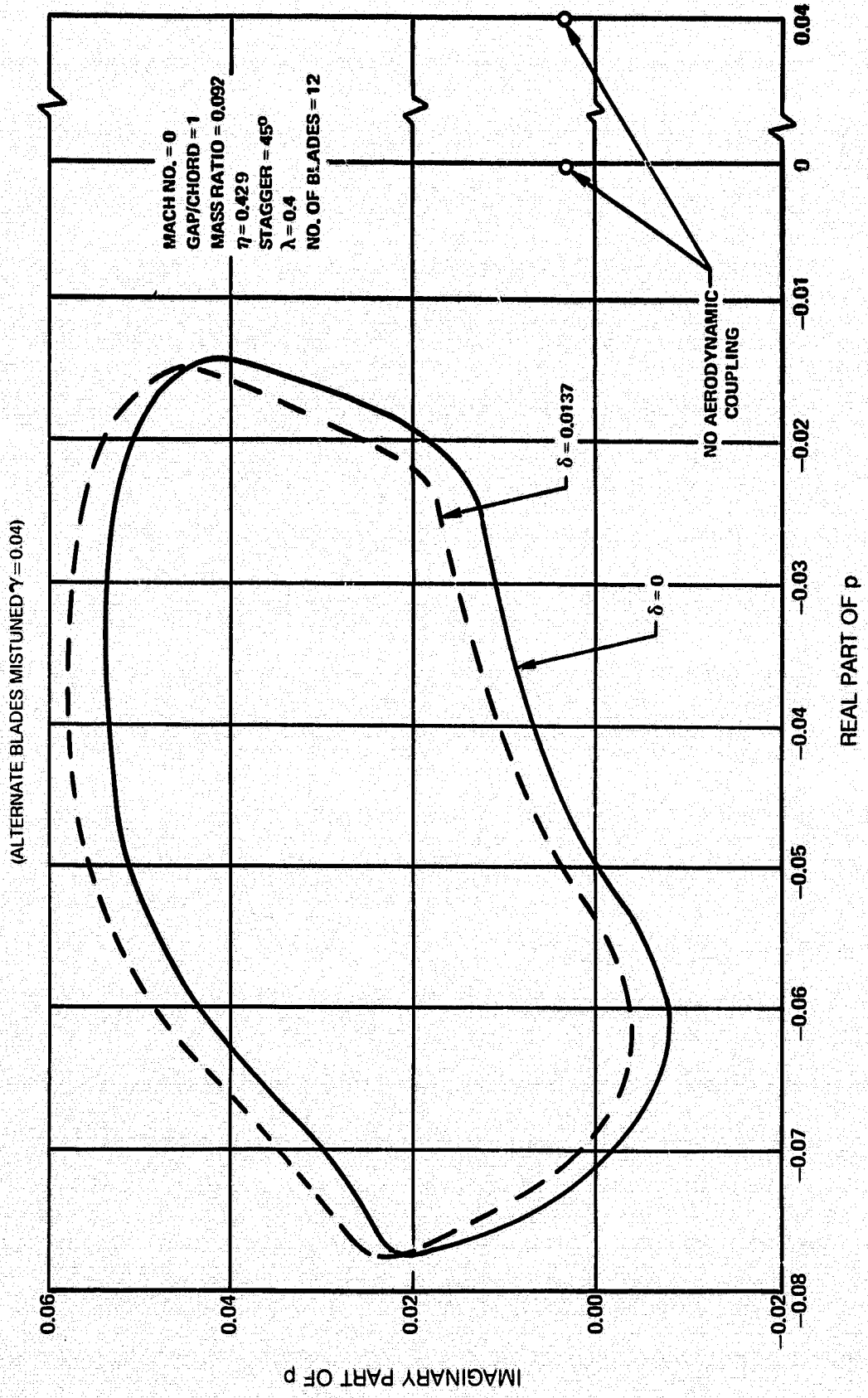
Figure 3 Effects of Mistuning on Blade Flutter

79—07—21—1

(SEE FIG. 2 FOR THE LOCUS OF EIGENVALUES)
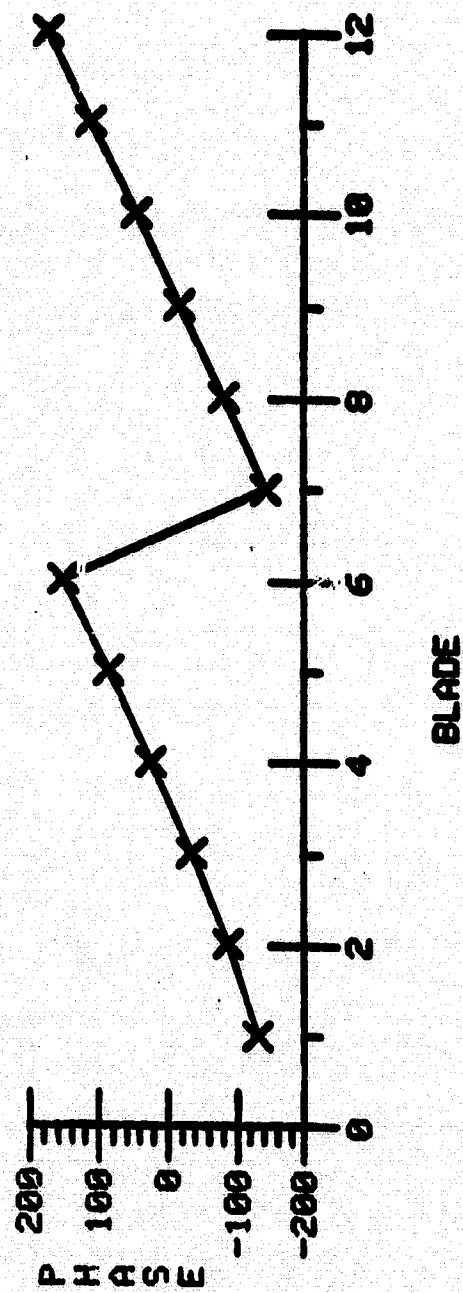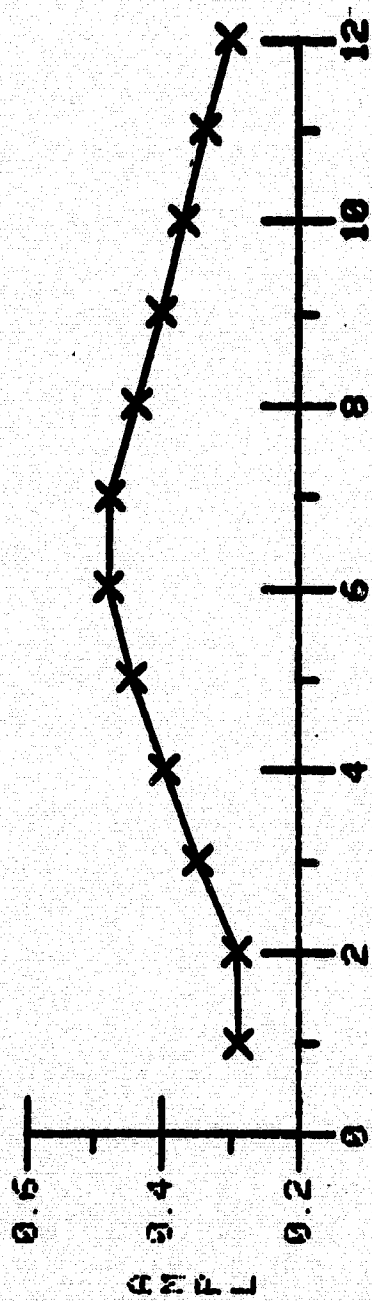
Figure 4 Eigenvector Associated with Eigenvalue p = − 0.0872 − i 0.0123
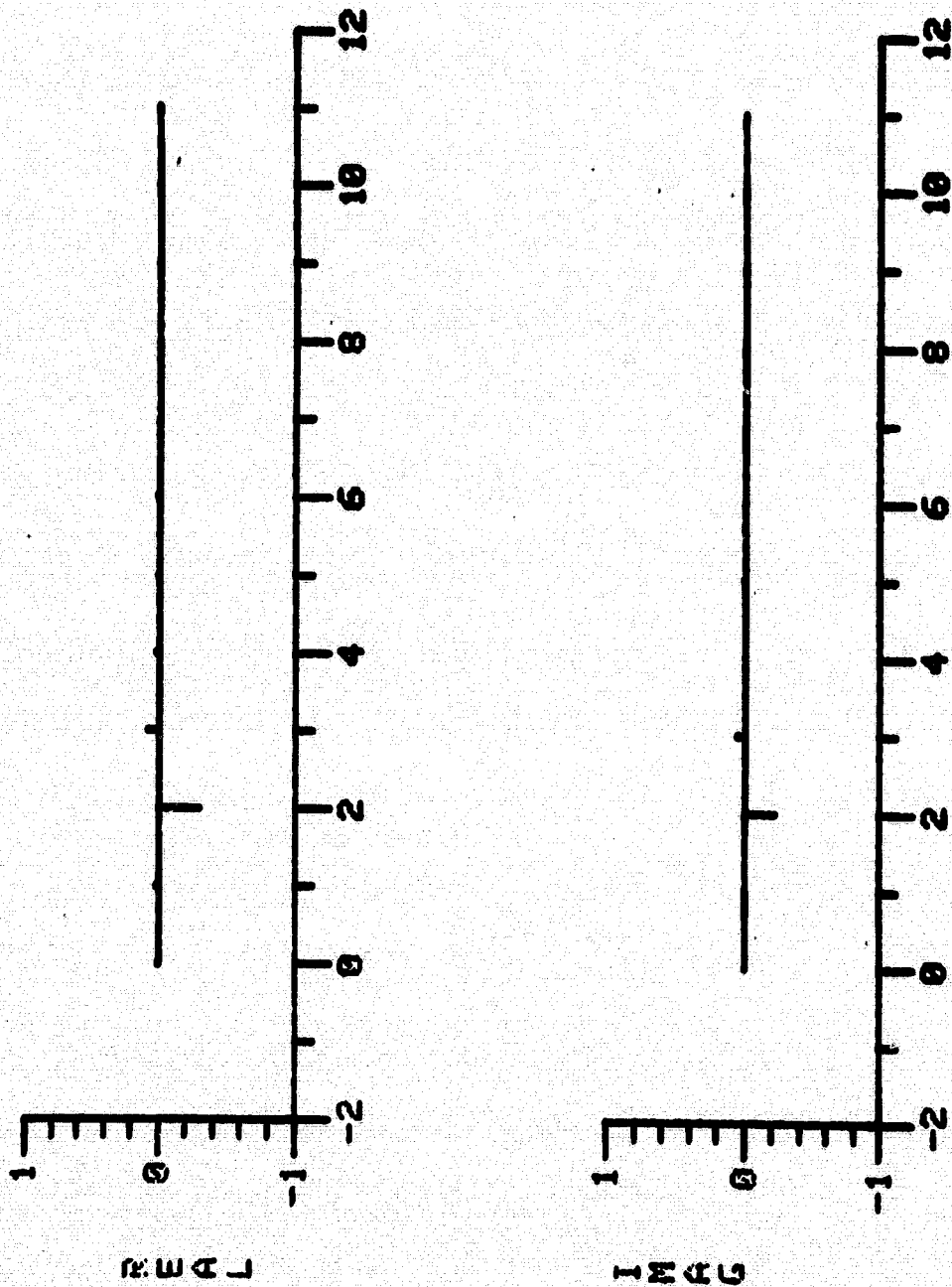
Figure 5 Strength of Harmonics Associated with Eigenvalue p = − 0.0872 − i 0.0123

HARMONIC
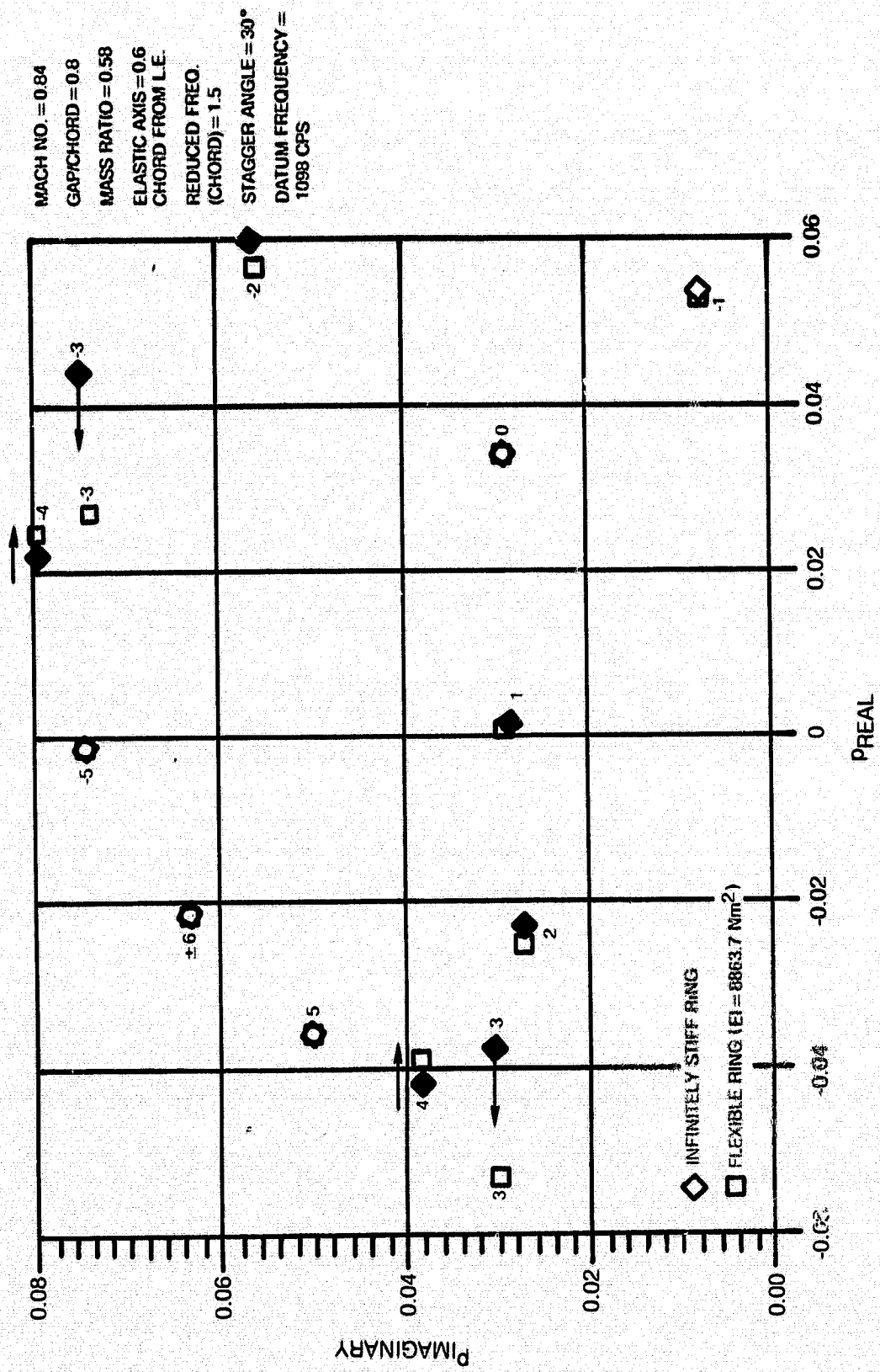
Figure 6 Eigenvalues for a 12 Bladed Tuned System

MACH NO. = 0.84
GAP/CHORD = 0.8
MASS RATIO = 0.58
ELASTIC AXIS = 0.6 CHORD FROM L.E.
REDUCED FREQ. (CHORD) = 1.5
STAGGER ANGLE = 30°
DATUM FREQUENCY = 1098 CPS

P_{REAL}

$P_{IMAGINARY}$

◇ INFINITELY STIFF RING
□ FLEXIBLE RING (EI = 8863.7 Nm²)
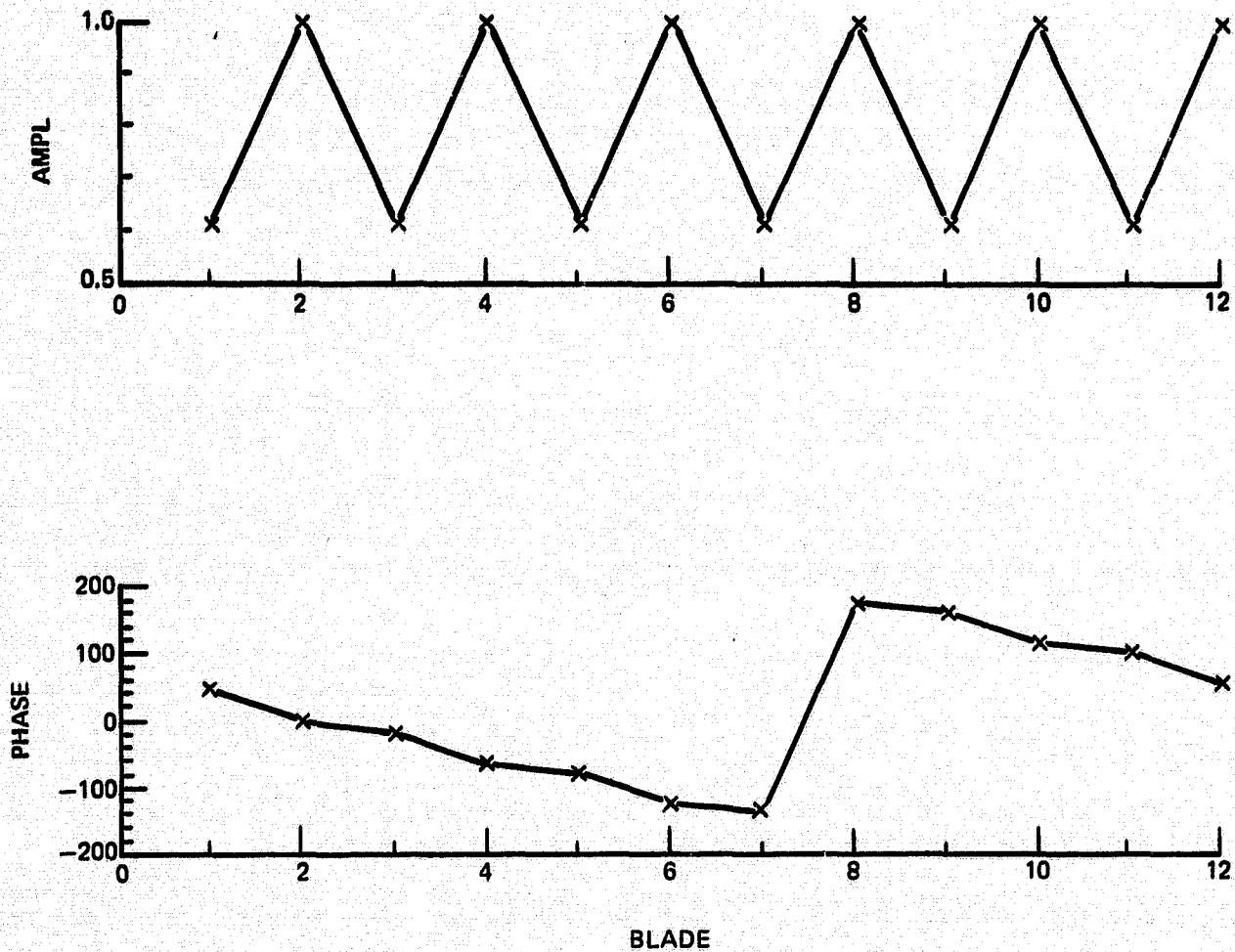
Figure 7   Eigenvector Associated with Eigenvalue $-0.0141 + i\,0.0406$

FAN CORRECTED AIRFLOW
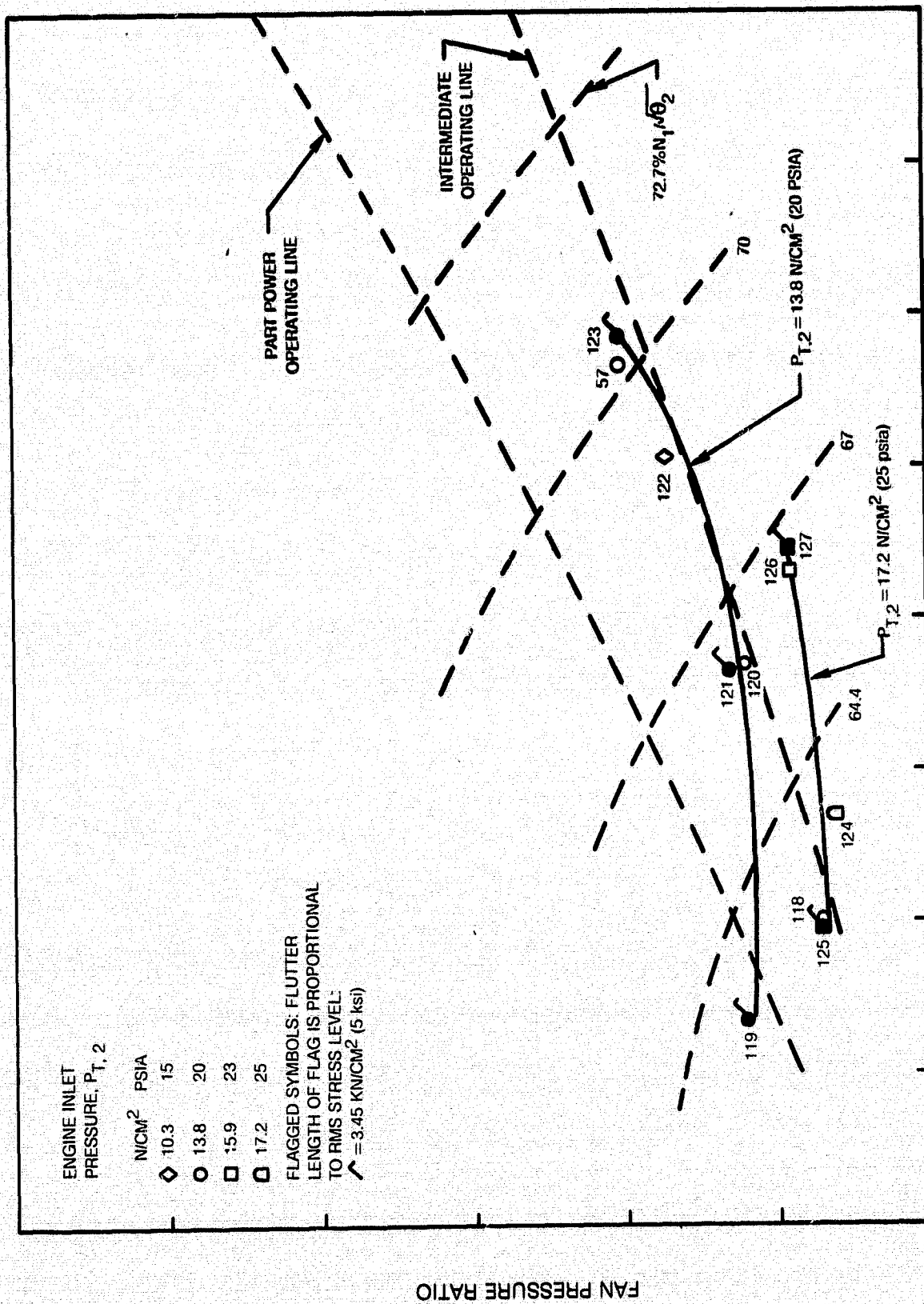
Figure 8 Fan First Rotor Subsonic Stall Flutter Boundaries

FAN PRESSURE RATIO

ENGINE INLET
PRESSURE, $P_{T,2}$

N/CM^2	PSIA
◇ 10.3	15
○ 13.8	20
□ 15.9	23
◻ 17.2	25

FLAGGED SYMBOLS: FLUTTER
LENGTH OF FLAG IS PROPORTIONAL
TO RMS STRESS LEVEL:
⌐ = 3.45 KN/CM² (5 ksi)

PART POWER
OPERATING LINE

INTERMEDIATE
OPERATING LINE

72.7% $N_1/\sqrt{\theta}_2$

$P_{T,2}$ = 13.8 N/CM² (20 PSIA)

$P_{T,2}$ = 17.2 N/CM² (25 psia)

70

67

64.4

57

123

122

127

126

121

120

124

118

125

119
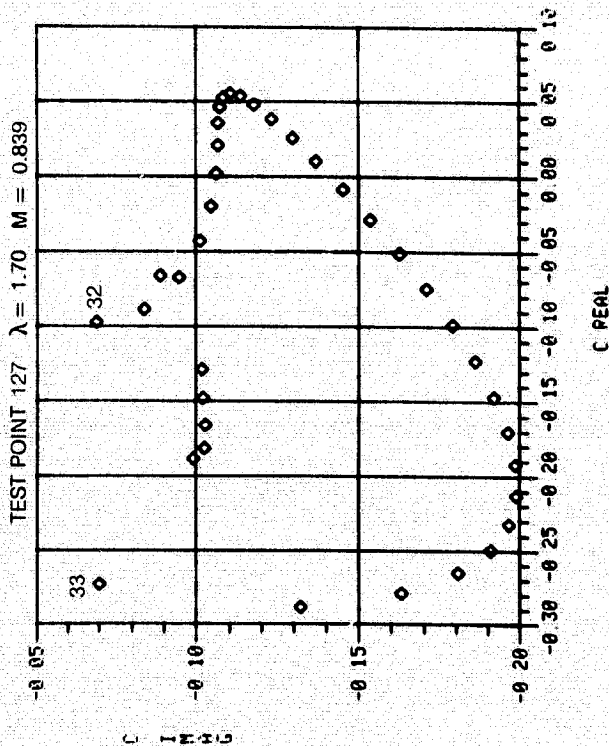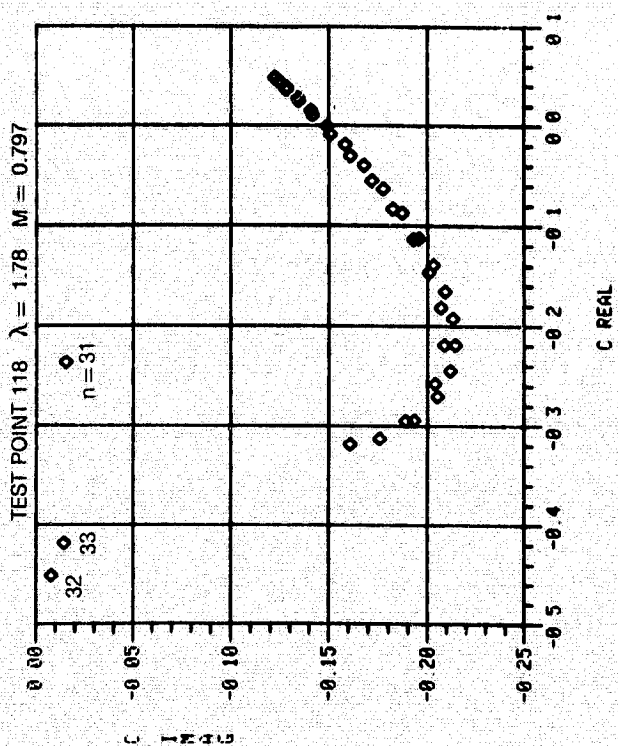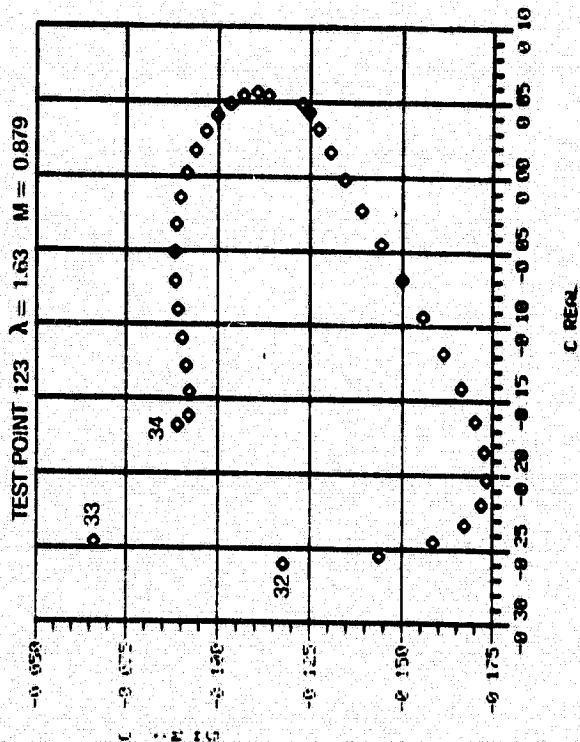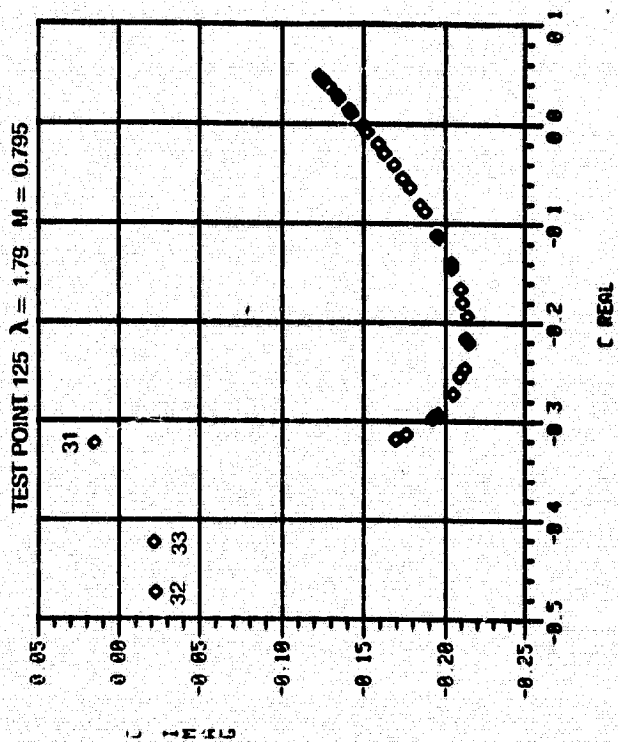
Figure 9 Unsteady Aerodynamic Coefficients
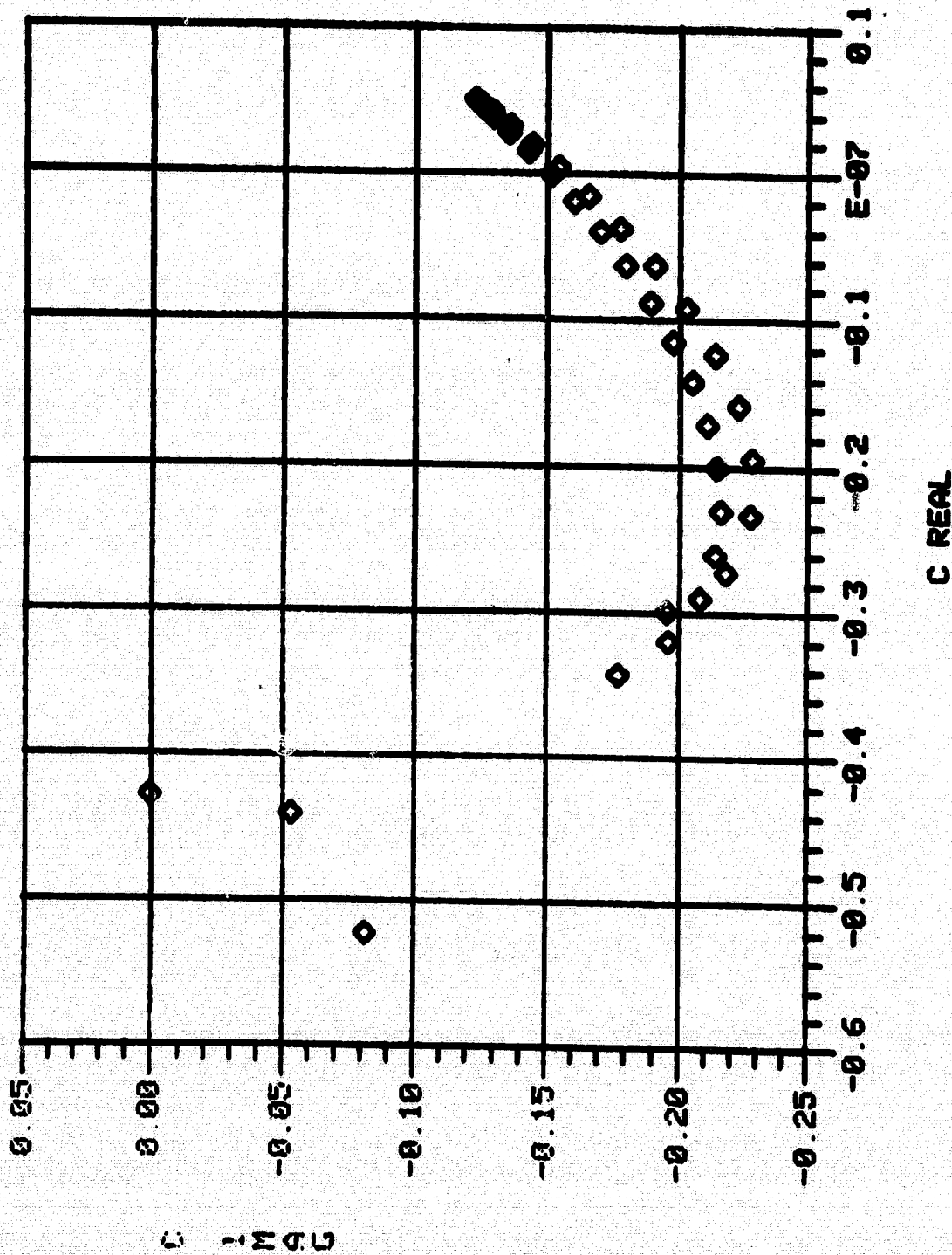
Figure 10 Unsteady Aerodynamic Coefficients (Four Collocation Points)

S/c = 0.8134   θ = 29°.75   λ = 1.790   M = 0.795   η = 0.440

C REAL
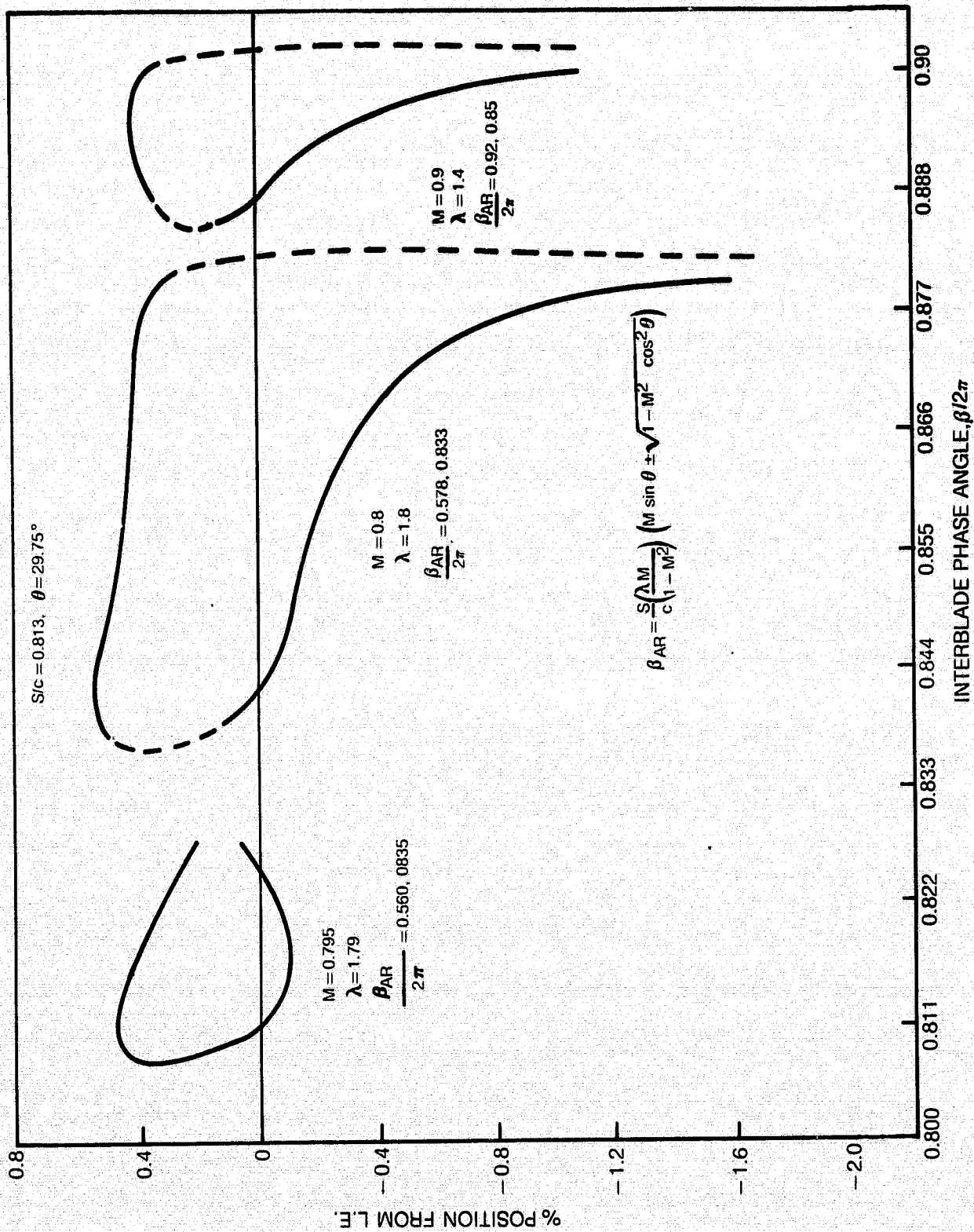
Figure 11 Acoustic Resonance Flutter

$S/c = 0.813, \quad \theta = 29.75°$

$M = 0.795$
$\lambda = 1.79$
$\dfrac{\beta_{AR}}{2\pi} = 0.560, 0.0835$

$M = 0.8$
$\lambda = 1.8$
$\dfrac{\beta_{AR}}{2\pi} = 0.578, 0.833$

$M = 0.9$
$\lambda = 1.4$
$\dfrac{\beta_{AR}}{2\pi} = 0.92, 0.85$

$\beta_{AR} = \dfrac{S}{c}\left(\dfrac{\lambda M}{1 - M^2}\right)\left(M \sin\theta \pm \sqrt{1 - M^2 \cos^2\theta}\right)$

INTERBLADE PHASE ANGLE, $\beta/2\pi$

% POSITION FROM L.E.

80—03—20—7
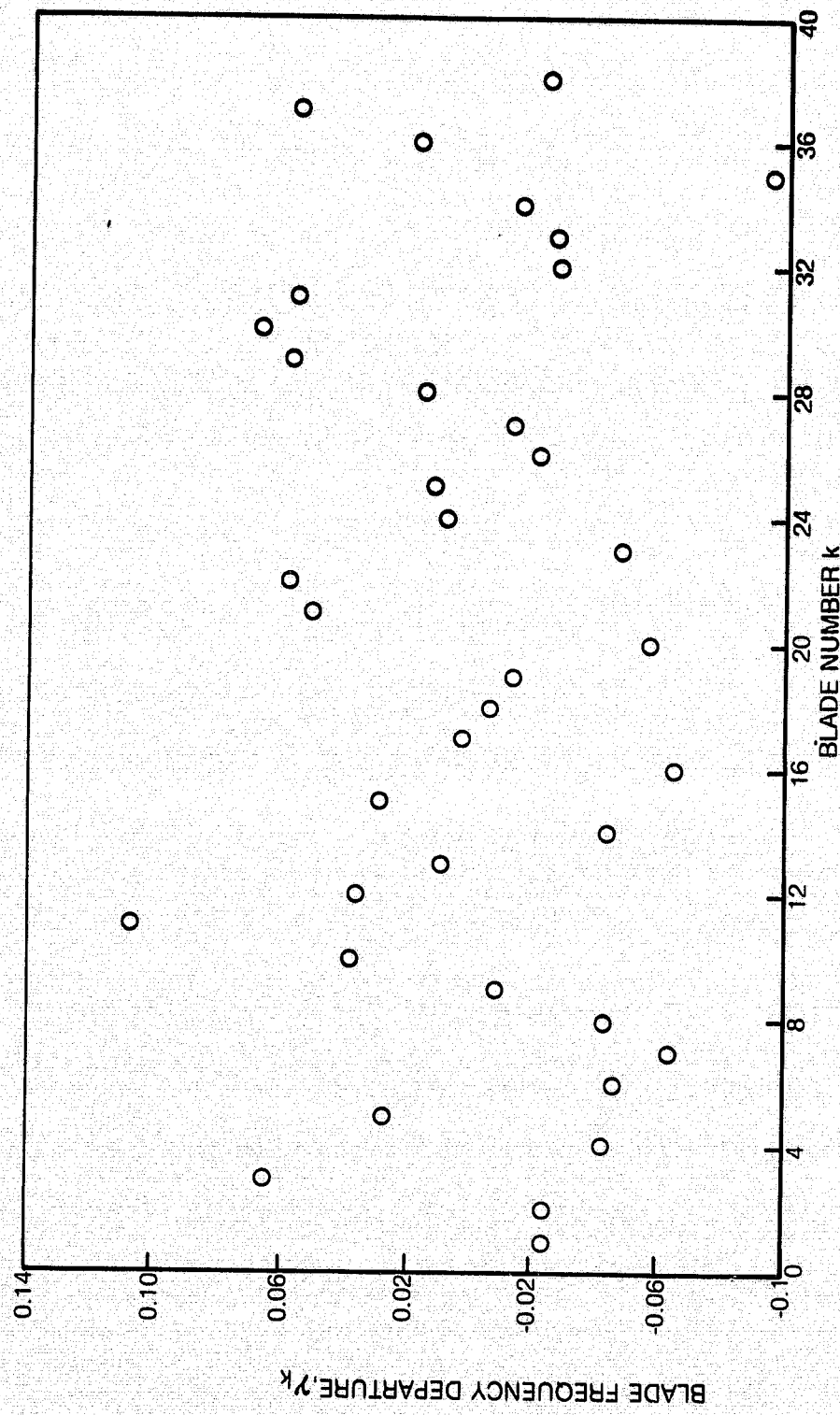
Figure 12 Departure of Individual Blade Frequencies from the Mean (γ_k)

BLADE FREQUENCY DEPARTURE, γ_k

BLADE NUMBER k
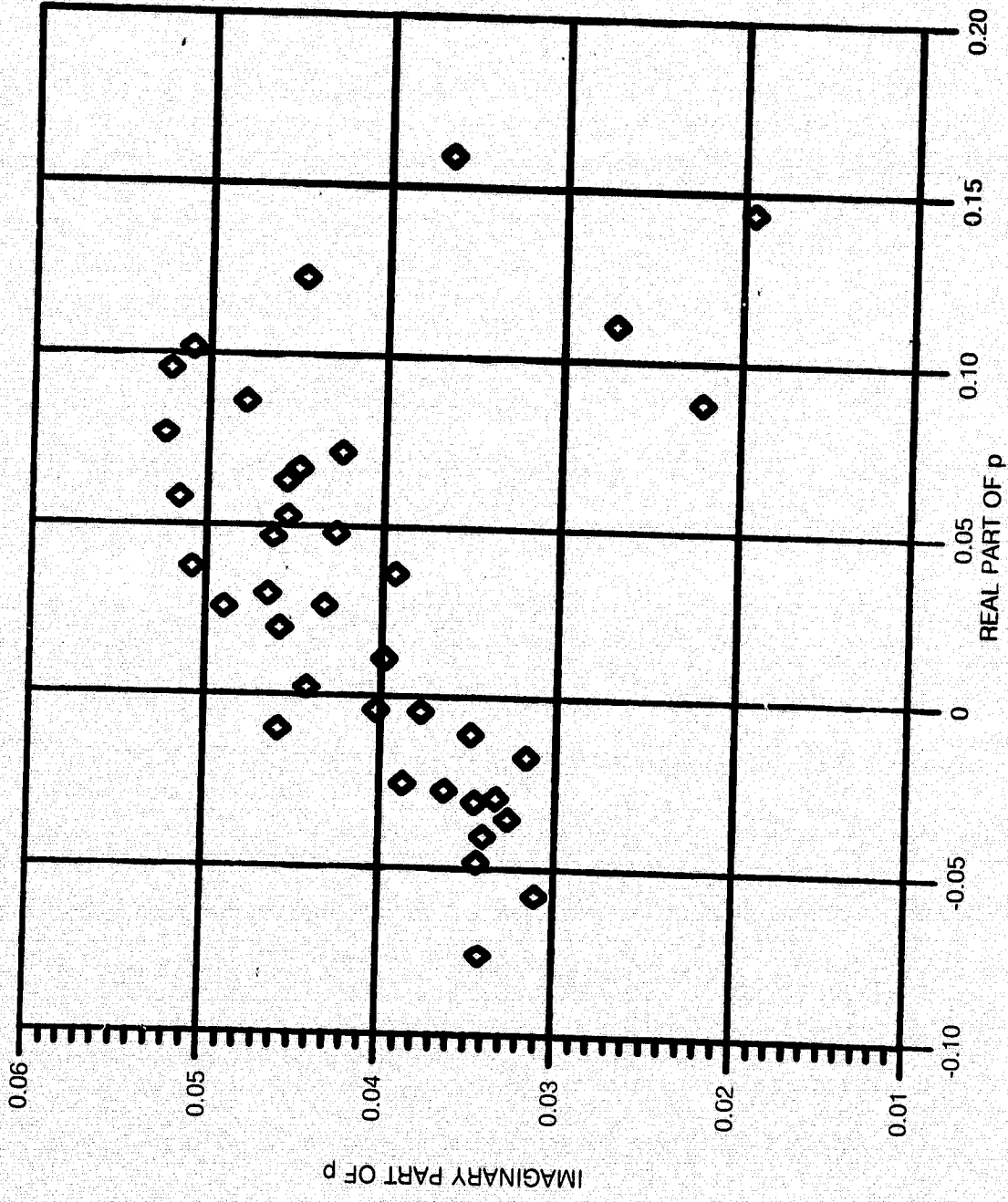
Figure 13 Effects of Mistuning on Blade Flutter Test Point 125

S/c = 0.8134
θ = 29.75°
η = 0.44
M = 0.795
λ = 1.79
μ = 0.76
N = 38

IMAGINARY PART OF p

REAL PART OF p

(SEE FIG. 13 FOR EIGENVALUES)
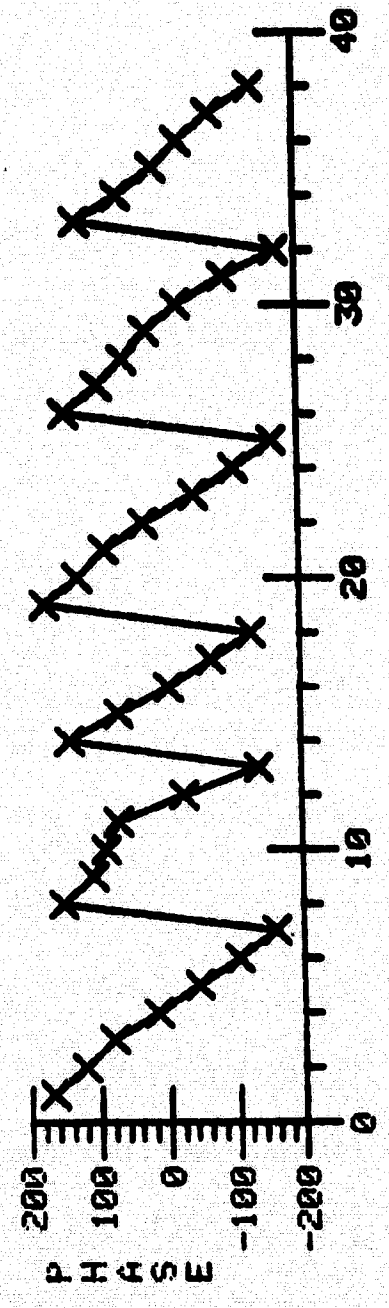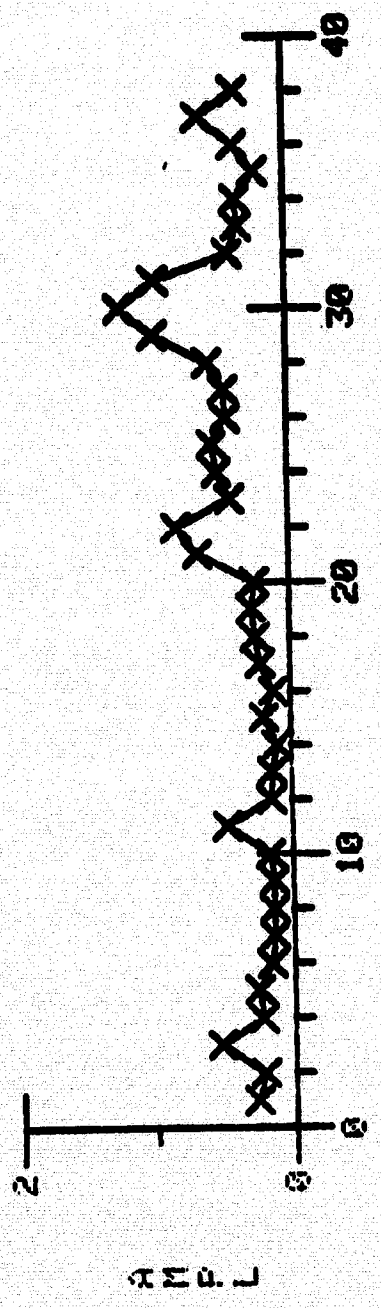
Figure 14 Eigenvector Associated with Eigenvalue 0.1436 + i.0195

BLADE
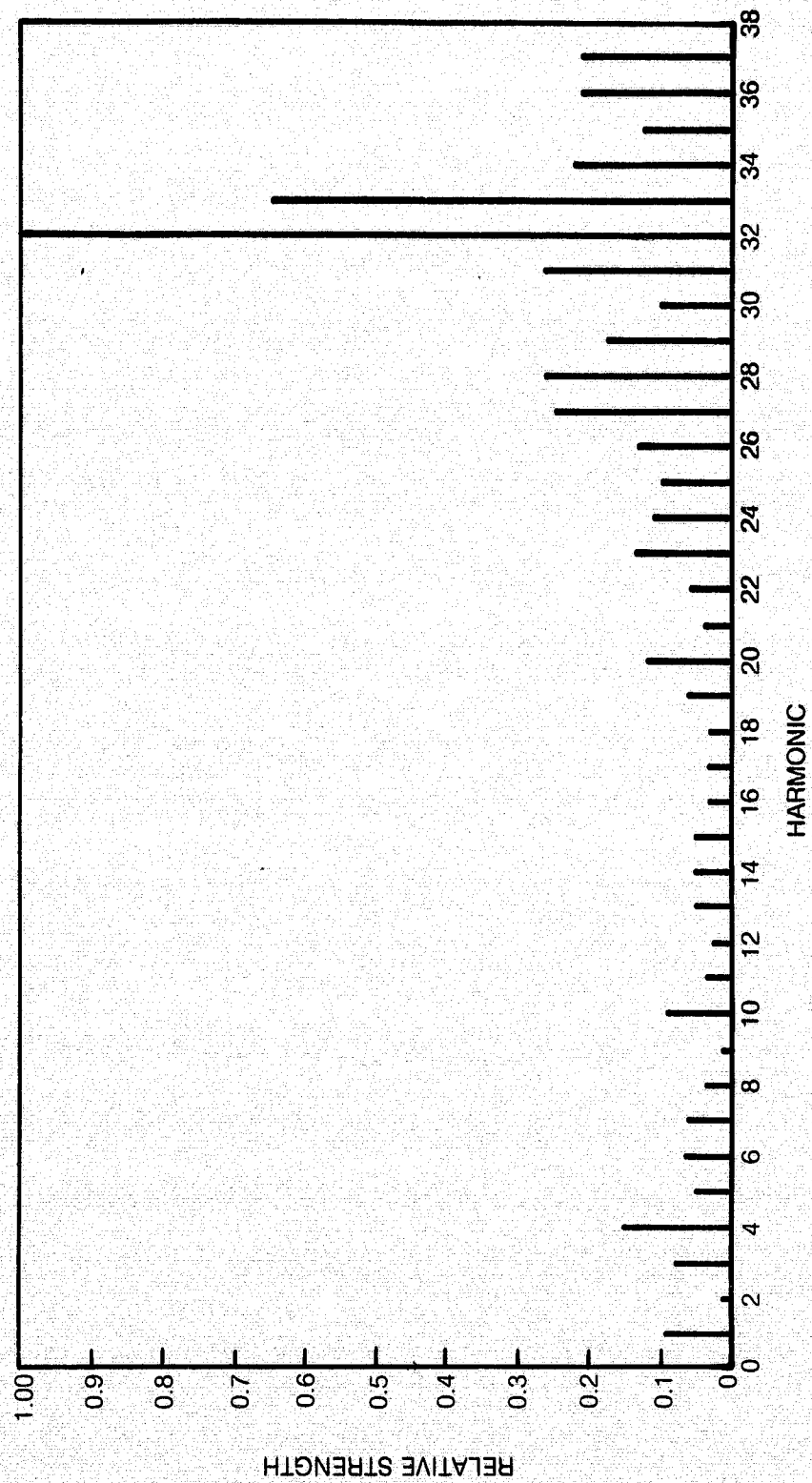
Figure 15 Strength of Harmonics Present in the Mistuned Mode at p = 0.1436 + i.0195
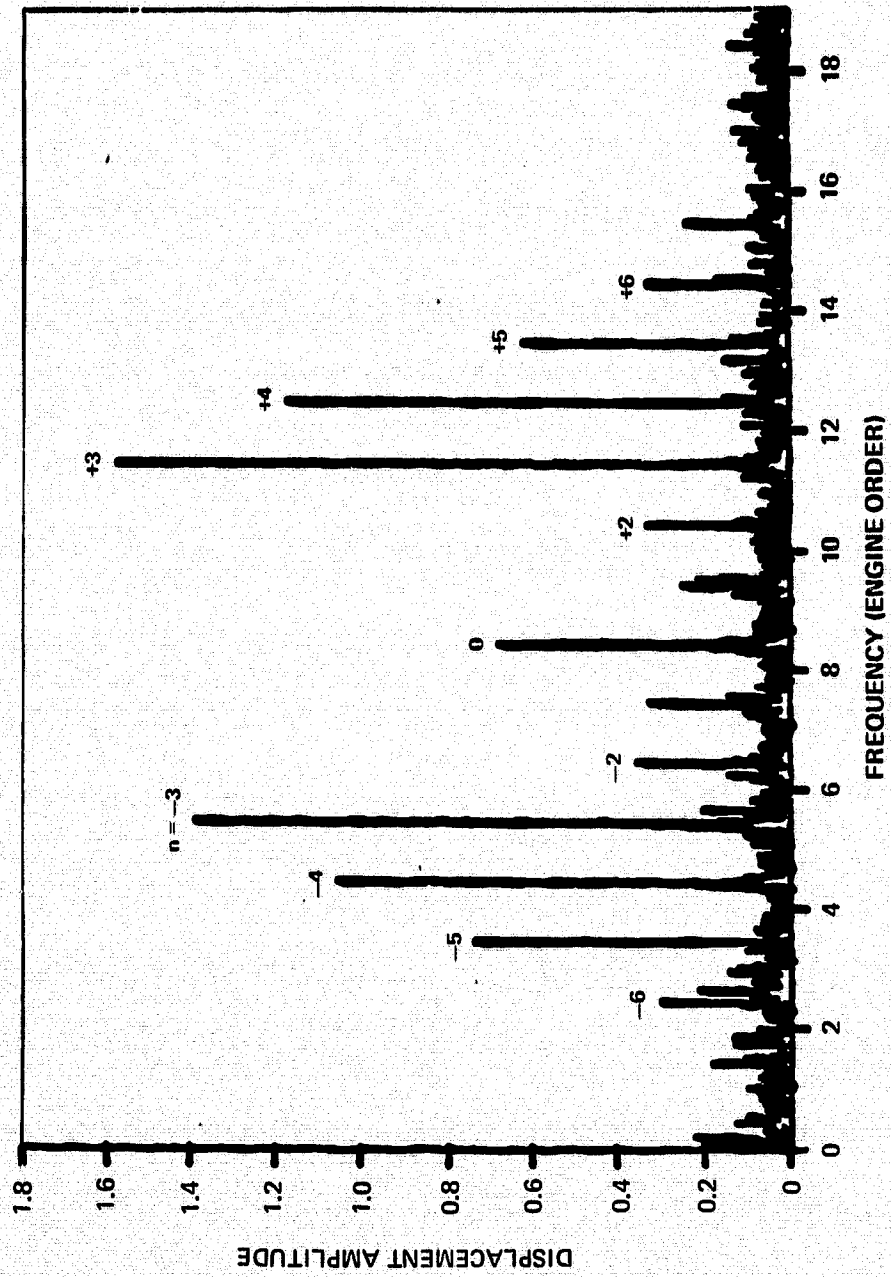
Figure 16 Displacement — Amplitude Spectrum
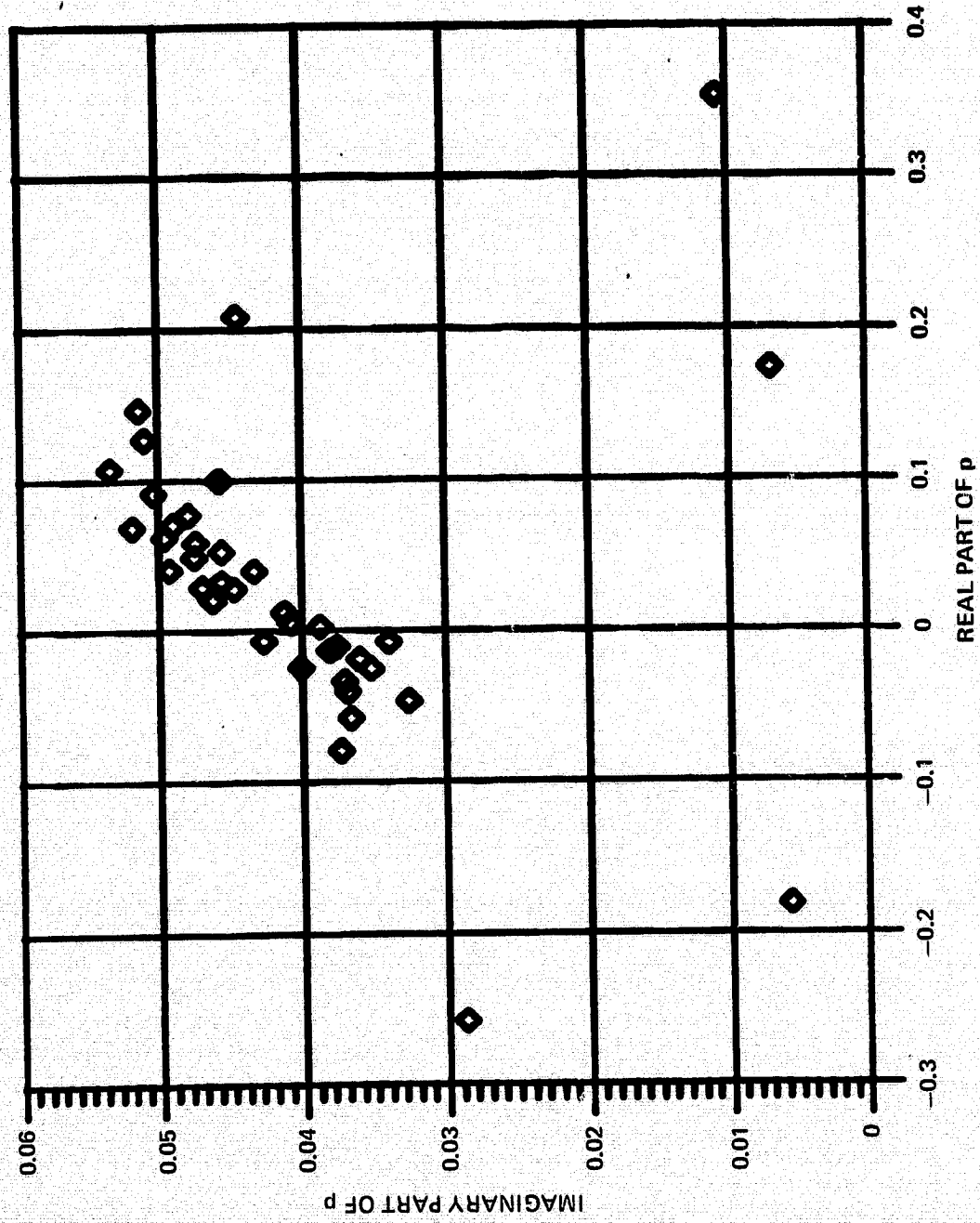
Figure 17 Mistuned Assembly with Aerodynamic and Mechanical Coupling (Test Point 125)

(SEE FIG. 17 FOR EIGENVALUES)
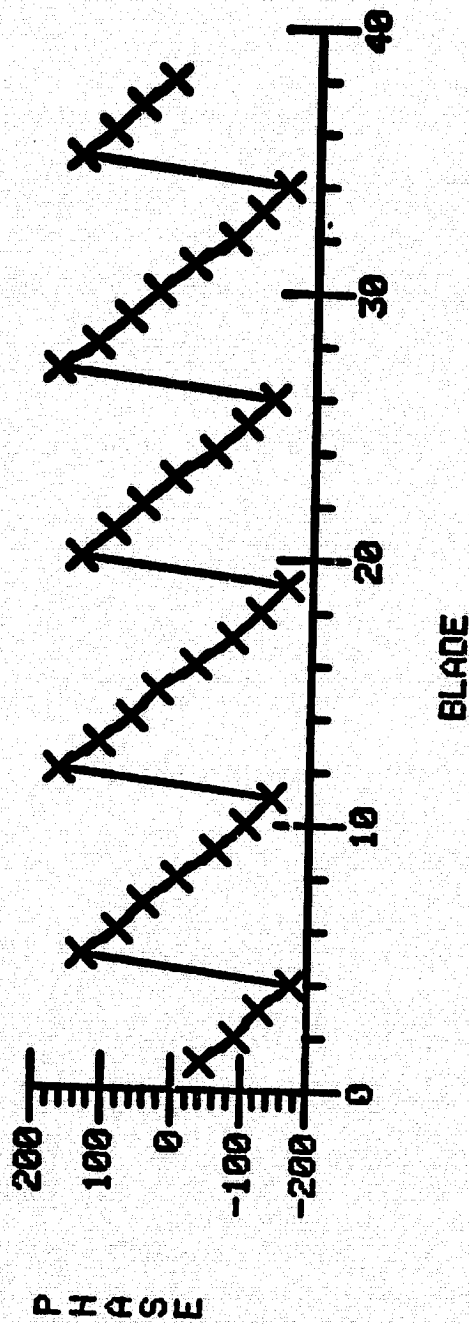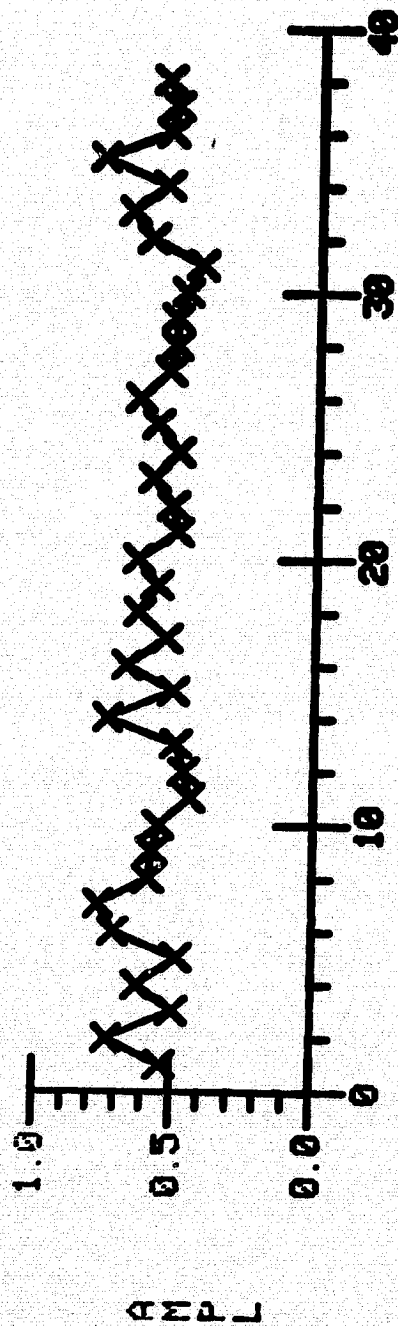
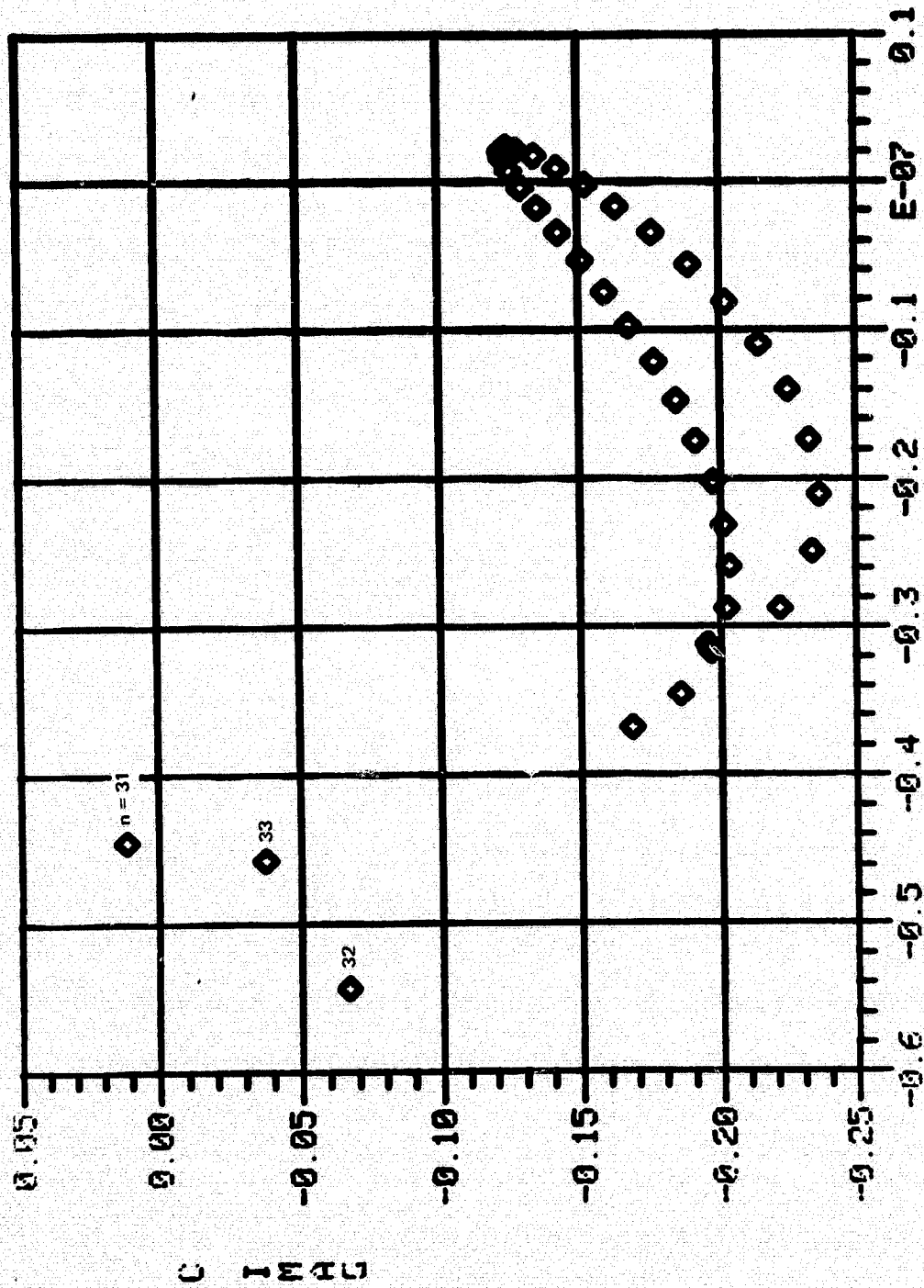Figure 18 Eigenvector Associated with Eigenvalue at p = -.1804+i.0057
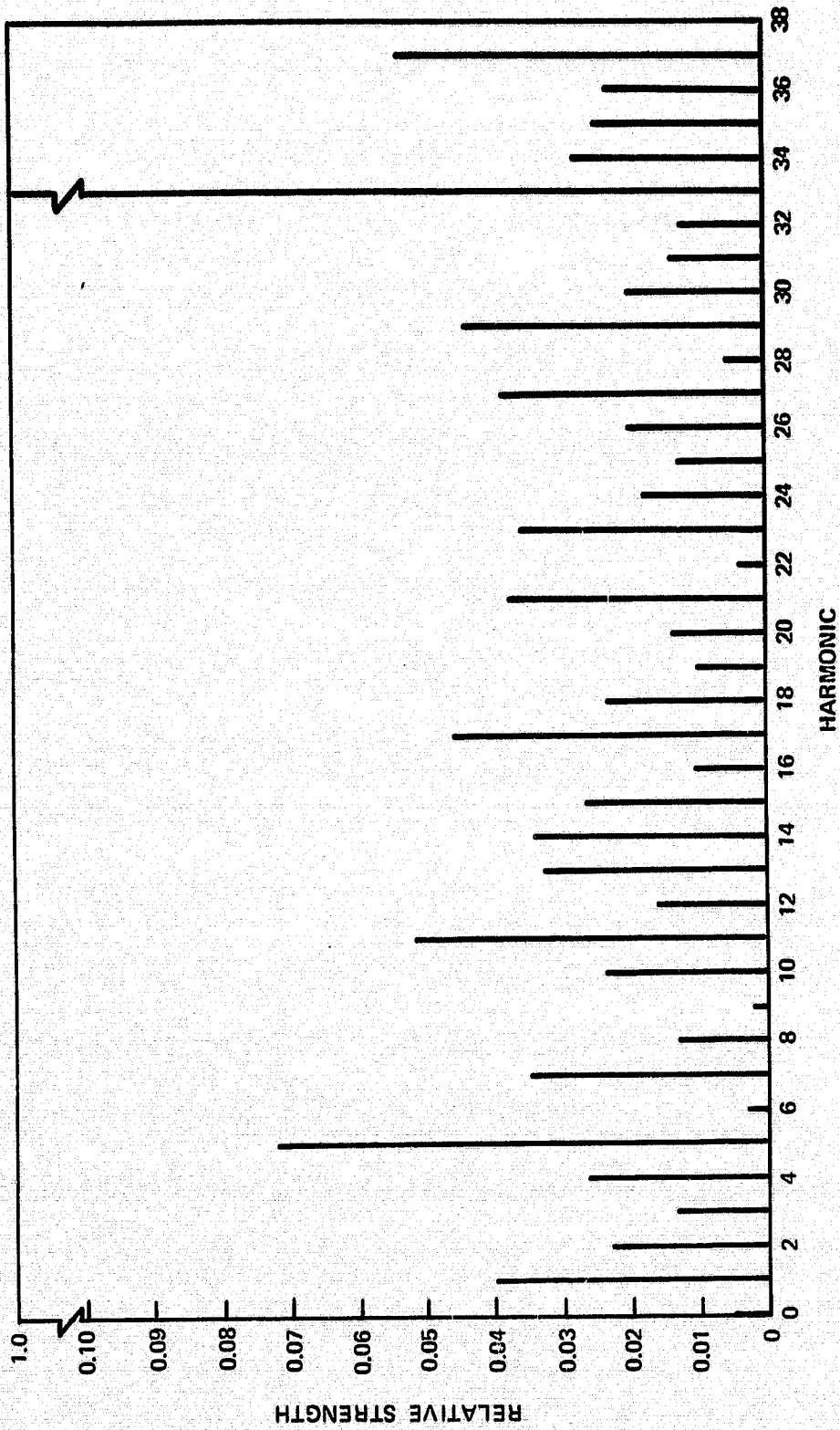
Figure 19 Strength of Harmonics Present in the Mistuned Mode at p = −.1804+i.0057
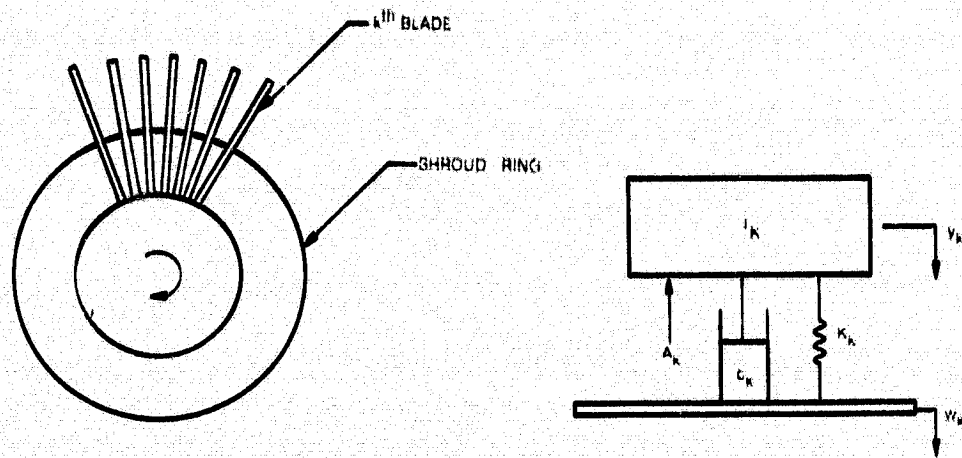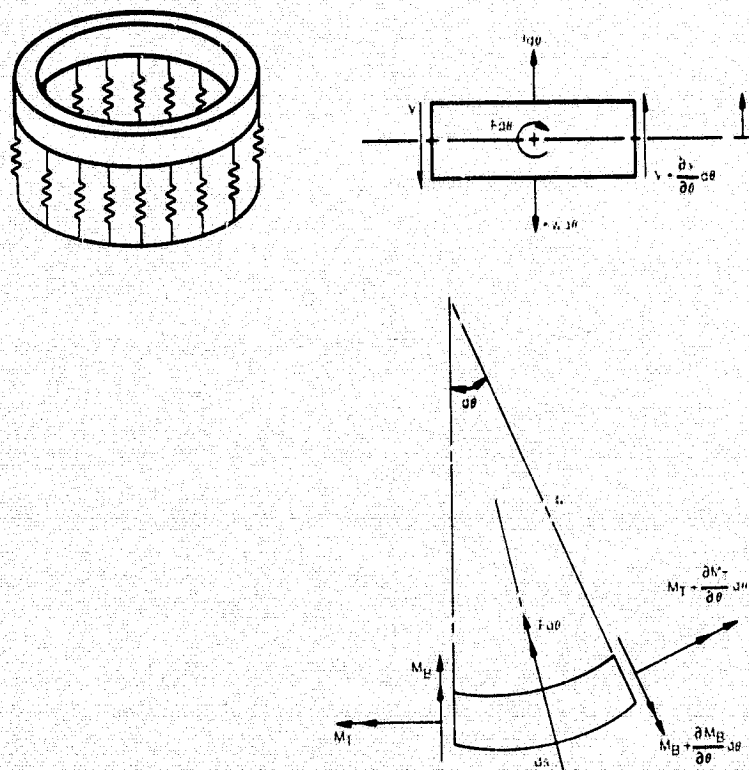
Figure 20 Unsteady Aerodynamic Coefficients

Figure 21 Analytical Model

Figure 22 "Shroud Ring" Model